POLITECNICO
MILANO 1863

SCUOLA DI INGEGNERIA INDUSTRIALE
E DELL'INFORMAZIONE

Development of a Portable Animal Ventilator for Hyperpolarized ^{129}Xe MRI and MRE at 9.4 Tesla

TESI DI LAUREA MAGISTRALE IN
BIOMEDICAL ENGINEERING - INGEGNERIA BIOMEDICA

Author: **Ludovica Nestore**

Student ID: 990501
Advisor: Prof. Raffaele Dellacà
Co-advisors: Prof. Thomas J. Royston, Davide Bizzotto, PhD
Academic Year: 2022-23

Abstract

As a non-invasive and powerful method for assessing lung function, hyperpolarized (HP) ^{129}Xe magnetic resonance (MR) imaging is increasingly being utilized in clinical settings to investigate various respiratory conditions. Concurrently, MR elastography (MRE) research holds promise in delivering crucial information regarding lung mechanical properties, particularly density and stiffness. Given the evolving nature of this field, numerous preclinical studies are still required. However, preclinical animal studies involving MRI and MRE encounter challenges such as the necessity for anesthesia, the need for precise delivery of very small tidal volumes (which affects gas administration accuracy), motion artifacts stemming from irregular breathing patterns during spontaneous respiration, and the demand for a high spatial resolution to detect regional changes.

To surmount these limitations, this project proposes a portable HP gas ventilator that enables high-resolution 3D imaging of dissolved and gas-phase ^{129}Xe in the lungs, compatible with a 9.4 Tesla MR system. The ventilator incorporates differential pressure transducers and a 3D-printed pneumotachometer, allowing for precise control of tidal volume, breathing cycles, and calibrated positive expiratory pressure in intubated animals. By leveraging low-cost microcontrollers, 3D-printed components, and open-source software, in addition to recapturing expelled HP gases, the overall cost per study is significantly reduced.

The device is adaptable for use with various small animals, including rats, mice, guinea pigs, and rabbits, obviating the need for tracheotomy and substantially improving post-study survivability. Anesthesia is integrated into the oxygen supply, enabling prolonged testing durations while minimizing invasiveness.

Future advancements will encompass the integration of the forced oscillation technique (FOT), thereby examining whether the combined utilization of MRI, MRE, and FOT can provide enhanced insights into complex lung function.

Keywords: Lung, Animal Ventilator, MRE Elastography, Stiffness, Hyperpolarized Gas

Abstract in lingua italiana

Come metodo non invasivo per valutare la funzione polmonare, l'imaging a risonanza magnetica (MR) con iperpolarizzazione del ^{129}Xe è sempre più utilizzato in ambienti clinici per investigare diverse condizioni respiratorie. Allo stesso tempo, la ricerca sull'elastografia a risonanza magnetica (MRE) è in grado di fornire informazioni cruciali riguardo alle proprietà meccaniche dei polmoni, in particolare la densità e la rigidità. Dato il carattere in evoluzione di questo campo, sono ancora necessari numerosi studi preclinici. Tuttavia, gli studi preclinici sugli animali che coinvolgono la MRI e la MRE incontrano sfide come la necessità di anestesia, la precisa erogazione di volumi correnti molto piccoli (che influisce sull'accuratezza dell'administrazione di gas), artefatti dovuti a movimenti derivanti da pattern di respirazione irregolare durante la respirazione spontanea e l'esigenza di un'alta risoluzione spaziale per rilevare cambiamenti regionali. Per superare queste limitazioni, questo progetto propone un ventilatore portatile per gas iperpolarizzato che consente l'imaging 3D ad alta risoluzione del ^{129}Xe disciolto e in fase gassosa nei polmoni, compatibile con un sistema MR da 9,4 Tesla. Il ventilatore incorpora trasduttori di pressione differenziale e un pneumotacometro stampato in 3D, consentendo un preciso controllo del volume corrente, dei cicli respiratori e della pressione espiratoria positiva calibrata negli animali intubati. Sfruttando microcontrollori a basso costo, componenti stampati in 3D e software open-source, oltre a catturare nuovamente i gas a iperpolarizzazione espulsi, il costo complessivo per studio viene significativamente ridotto. Il dispositivo è adattabile all'uso con vari piccoli animali, tra cui ratti, topi, porcellini d'India e conigli, evitando la necessità di tracheotomia e migliorando sostanzialmente la sopravvivenza post-studio. L'anestesia è integrata nell'apporto di ossigeno, consentendo durate di test prolungate riducendo al minimo l'invasività. Gli sviluppi futuri comprenderanno l'integrazione della tecnica di oscillazione forzata (FOT), esaminando quindi se l'utilizzo combinato di RM, MRE e FOT possa fornire approfondimenti migliorati sulla complessa funzione polmonare.

Parole chiave: Polmoni, Ventilatore Meccanico, Risonanza Magnetica, Elastografia

Contents

Introduction and Motivation

0.1.   The Necessity of new lung imaging techniques

Numerous pulmonary pathologies can significantly impact the structure and mechanical characteristics of lung tissue, leading to alterations in airway geometry, tissue stiffness (elasticity), and overall gas exchange efficiency within the alveoli. These pathologies can either reduce the effective surface area available for gas exchange or impede respiration by causing fibrosis (stiffening) of the lung tissue.

There exists a pressing and immediate necessity for the development and implementation of enhanced noninvasive imaging techniques that do not involve ionizing radiation. These techniques should be capable of accurately quantifying both regional gas exchange efficiency and the intrinsic mechanical properties of lung tissue, particularly in cases where diffuse or localized fibrosis or tumors have caused notable alterations.

Conventional magnetic resonance imaging (MRI) based on water (proton) signals performs poorly in the lungs due to air presence and tissue/air boundaries. Hyperpolarized (HP) ^{129}Xe(non) MRI shows promise in regionally quantifying ventilation and gas exchange efficiency. The degradation of gas exchange efficiency, which often manifests as chronic shortness of breath, is a distinguishing characteristic of Post-Acute Sequelae of SARS-CoV-2 infection (PASC) or "long" COVID [6]. Therefore, the development and implementation of new lung imaging techniques are crucial not only for addressing the broader challenges posed by pulmonary pathologies but also for understanding and managing the long-term effects of COVID-19.

Conversely, MR elastography (MRE) stands as a non-invasive phase-contrast magnetic resonance (MR) technique with the capacity to provide crucial insights into the mechanical properties of the lung, specifically by enabling the creation of quantitative maps depicting the stiffness of soft tissue. However, the effectiveness of conventional proton-based MRE in the context of the lungs is limited, as previously discussed. Nonetheless, a novel approach emerges through the utilization of hyperpolarized (HP) ^{129}Xe MRI which represents a pioneering application for MRE.

By integrating MRE with HP ^{129}Xe MRI, researchers and medical professionals gain the ability to circumvent the challenges posed by traditional proton-based MRE techniques when applied to lung imaging. This innovative combination allows for the acquisition of previously unattainable information regarding the mechanical characteristics of lung tissue, especially the comprehensive assessment of soft-tissue stiffness throughout the lungs, opening up new avenues for studying lung pathologies, monitoring disease progression, and optimizing treatment strategies.

0.2.   Thesis goal

The field of Xenon Imaging techniques is rapidly expanding, yet further preclinical studies are imperative to advance our knowledge in this area. However, there are several challenges encountered in conducting preclinical animal studies utilizing magnetic resonance imaging (MRI) and MR elastography (MRE), which must be addressed. These challenges include:

- Controlling very small tidal volumes: Precise control over the ventilation of small volumes in animal subjects is required to ensure accurate and reliable data acquisition during imaging studies.

- Anesthesia requirement: Anesthesia is necessary to immobilize the animals during imaging procedures. However, it introduces complexities, such as potential impacts on respiratory patterns, and the balancing of anesthesia administration with oxygen supplementation, which need to be carefully considered and mitigated.

- Motion artifacts during spontaneous breathing: Spontaneous breathing in animals can lead to motion artifacts, which may affect the quality and accuracy of the imaging data obtained. These artifacts need to be minimized or eliminated to ensure reliable results.

- High spatial resolution for detecting regional changes: Achieving high spatial resolution is crucial to accurately detect and analyze regional changes in lung morphology and mechanics. This requirement adds an additional level of complexity to preclinical imaging studies.

To overcome these limitations, to the best of our knowledge, the optimal strategy involves mechanically ventilating the animal subjects using positive pressure ventilation. This approach allows for precise control over ventilation parameters, minimizing motion artifacts and maintaining consistent and reproducible breathing patterns. Additionally, performing full 3D encoding incrementally over multiple breathing cycles while suspending

respiratory motion further enhances the accuracy and reliability of the acquired data.

Hence, the project offers several notable advantages, including

1. The development of a portable HP gas ventilator that allows for high-resolution 3D imaging of dissolved and gas-phase ^{129}Xe in the lungs, compatible with the 9.4 Tesla preclinical MRI system.

2. Significantly improved post-study survivability of animals by eliminating the need for tracheostomy. This eliminates potential complications associated with invasive procedures, enhancing the welfare and ethical considerations in animal research.

3. Creation of a cost-effective system that is readily reproducible and adaptable to various small animal models. The low-cost nature of the device enhances accessibility and promotes broader adoption in preclinical research settings.

4. Implementation of a novel device that integrates magnetic resonance (MR) imaging, MR elastography, and Force Oscillation Technique (FOT) for the first time. This multifaceted approach allows a comprehensive assessment of lung mechanics and provides valuable insights into both structural and functional aspects of lung health and disease.

0.3. Outline

The thesis follows a well-structured organization, with each chapter addressing specific aspects of the research. The outline of the thesis is as follows:

- Chapter 2 serves as a comprehensive literature review, offering a discussion on the current state of the art in Xenon imaging. This chapter provides essential background knowledge and explores the fundamental principles underlying Xenon imaging techniques. It synthesizes existing research and establishes a solid foundation for the subsequent chapters.

- Chapter 3 focuses on the development of the ventilator and presents detailed methods and technical procedures employed in its construction. It begins by illustrating all the components involved in the ventilator design, highlighting their respective roles and functionalities. Additionally, this chapter delves into the codes that control and monitor pressures, as well as the management of tidal volume. A thorough exposition of the ventilator's design and operation is provided, ensuring a comprehensive understanding of the technical aspects involved.

- In Chapter 4, the validation process is extensively discussed. This chapter outlines

the rigorous testing and evaluation procedures conducted to ensure the reliability and accuracy of the developed ventilator.

- Chapter 5 engages in a detailed discussion of the obtained results. This chapter provides a comprehensive and critical analysis of the outcomes, offering insights into the implications and potential applications of the research findings.

- Chapter 6 examines the limitations encountered throughout the project. It critically evaluates the challenges, constraints, and potential shortcomings that may have affected the research outcomes. Additionally, this chapter explores avenues for future implementation and improvement of the project, discussing potential areas for further exploration and development. It offers a forward-looking perspective, outlining potential strategies to overcome limitations and enhance the project's impact in future studies.

The structured organization of the thesis allows for a systematic and comprehensive exploration of the research topic. Each chapter contributes to a cohesive narrative, providing a well-rounded understanding of the research process, results, and future directions.

1 | Background

The objective of this chapter is to provide the reader with the essential theoretical background knowledge that facilitates a better understanding of the issues addressed and the rationale behind the decisions made during ventilator development. The chapter is organized as follows:

Sections 2.1 and 2.2 provide an introduction to the fundamental principles of MR Elastography (MRE), with a specific focus on the innovative approach of lung hyperpolarized gas MRE. These sections aim to familiarize the reader with the basics of MRE and highlight the novel application of this technique in lung imaging.

Section 2.3 delves into Xenon Imaging techniques, offering an in-depth exploration of the properties of Xenon (Xe) and providing an overview of the current state of the art in this field.

Section 2.4 presents the challenges associated with animal studies in the current research landscape. This section sheds light on the complexities and difficulties encountered when conducting studies involving animals, particularly in the context of Xenon Imaging techniques.

Finally, Section 2.5 emphasizes the overarching goal of the project. This section explicitly states the primary objective of the research and underscores its importance.

1.1. Stiffness as a Biomarker to assess Lung Mechanics

Lung function and its ability to deform are strongly interconnected, chronic respiratory diseases such as asthma, fibrosis, and pulmonary hypertension result in progressive morphological and mechanical alteration of the lung[7].

In the field of medical research, the assessment of *in vivo* lung stiffness has long been recognized as a promising biomarker for the early detection and diagnosis of various lung diseases. This parameter offers valuable insights into lung mechanics, including

characteristics such as elasticity and compliance.

This metric represents the amount of resistance the lungs experience while breathing: the increase in lung stiffness, causes a decrease in lung compliance thus breathing required more effort. It changes can be an early indicator of the occurrence of a disease or the effectiveness of a treatment, allowing doctors to intervene promptly. Therefore, it cannot be overstated how important lung stiffness is in clinical practice and research. It is a vital biomarker that plays a crucial role in the diagnosis, management, and treatment of various lung diseases.

1.2.   Lung MR Elastography

The National Heart, Lung, and Blood Institute of the National Institutes of Health recognizes the pressing need for non-invasive techniques that can effectively and spatially resolve the inherent mechanical properties of the lung [1], since techniques such as Conventional X-ray imaging and CT provide only anatomical and morphological information about the extent of the disease. MR elastography (MRE) is an emerging technique that has shown great promise in accessing elastic properties of tissue-like materials [15], without any need for biopsy.

It is a non-invasive phase-contrast magnetic resonance (MR) technique imaging technique that enables the assessment of soft-tissue stiffness by imaging propagating harmonic waves within the tissue. It involves three main components: an external driver for mechanical vibrations, an MRE pulse sequence for recording tissue movement and an inversion algorithm to determine stiffness information.

This method has several advantages over traditional techniques, including higher sensitivity and specificity, increased accuracy, and faster imaging times. The utilization of Magnetic Resonance Elastography (MRE) has demonstrated its efficacy in effectively assessing the mechanical characteristics of various organs, encompassing but not limited to the breast [19], brain [13], kidney [18], prostate [11], liver [17], and muscle [2]. This evaluation is contingent upon the presence of a signal-to-noise ratio (SNR) of significant magnitude, guaranteeing the preservation of phase stability.

In recent years, studies on lung MR Elastography have increased significantly due to improvements in inversion algorithms and the research of Fakhoury et in 2022 [4] led to several conclusions:

- Shear stiffness was substantially greater during free breathing than during a breath-hold, which may be caused by the lung parenchyma relaxing under stress or by

inconsistent breath-holds.

- As age, the lung's shear stiffness reduced, which may be related to a reduction in the compliance of the chest wall during free breathing.

- There is no observable difference in lung stiffness between males and females

Nevertheless, performing MRE in the lungs also has technical limitations:

First of all, because of the difference in the anatomical structure (ie, size and shape) and location between the right and left lung, the latter's shear stiffness may be significantly greater than the former's [4]. Furthermore, the left lung is subjected to cardiac-motion artifact, and in many types of research, only the right lung is scanned.

Secondly, a prominent obstacle in Magnetic Resonance Elastography (MRE) arises from its reliance on proton-based principles. This inherent characteristic gives rise to a relatively diminished signal-to-noise ratio (SNR) within the lung parenchyma, where the spin density is typically around 0.2–0.3 g/cm^3, in contrast to the 1.0 g/cm^3 observed in water. Additionally, the microstructural composition of lung tissues induces pronounced T*2 effects, further exacerbating the deterioration of lung magnetic resonance (MR) image quality [14].

Furthermore, in the research of Martinelli et al. in 2017 it is shown that evaluating stiffness at TLC is very challenging since the increased volume of air in the lung lobes reduces the effective lung density and further lowers SNR[8].

1.2.1. Hyperpolarized Gas MRE

To tackle this challenge, a novel approach involves the utilization of hyperpolarized noble gas as a contrast agent, which can encode shear wave displacement within its phase. The groundbreaking study conducted by Goss et al. in 2006 [5] provides the initial evidence demonstrating that polarized noble gases offer a distinctive means to assess lung shear stiffness, structure, and function.

The researchers established that instead of relying on the local supporting structures, an entrapped polarized gas can serve as a medium for storing bulk phase changes generated by the concurrent application of motion-sensitizing gradients and cyclic shear motion. Furthermore, the introduction of hyperpolarized noble gases allows for a substantial increase in signal, at least four orders of magnitude higher than the magnetic resonance (MR) signal obtained when the gas is in thermal equilibrium [14]. It is worth noting that during transportation, the polarization of the gas was reduced by 50%. Nevertheless, even with 50% polarization, ^{3}He can achieve approximately a twofold signal increase compared

to conventional ^{1}H imaging, considering an estimated reduction in spin density 3.5410^{-4} atoms/cm^3 for a comparable ^{3}He Volume(at 1-bar and 310K) in comparison to ^{1}H [10].

This notable improvement, coupled with the ability to employ ultrashort-TR (repetition time) imaging sequences due to the absence of T1 relaxation effects in ^{3}He, facilitates a substantial reduction in imaging time. Consequently, it becomes feasible to acquire multiple wave images during a single, brief breath-hold, expanding the potential application of this technique to patients suffering from lung diseases.

In conclusion, hyperpolarized MR elastography is an essential imaging technique for accessing lung mechanics. This method enables early detection and improved management of lung diseases by giving clinicians useful information on lung stiffness, compliance, and ventilation. Hyperpolarized MR elastography has the potential to revolutionize the diagnosis and treatment of lung diseases and improve patient outcomes.

1.3.   Introduction to Xenon Imaging

However, research on the hyperpolarized gas MRE to resolve lung mechanics is just getting started, whereas Hyperpolarized (HP) inert gas MRI has become a new diagnostic tool for assessing regional gas exchange [22].

This technique involves the inhalation of a hyperpolarized gas, such as Helium-3 or Xenon-129, which is then imaged using MRI. HP inert gas MRI has several advantages over traditional imaging techniques, including, improved sensitivity, and the ability to detect early changes in lung function. As it has already been said, conventional Lung MRI is extremely challenging because of the low proton density in the lungs, resulting in a low SNR. While in the other organs that have large water components, the largest contribution to the signal intensity is given by the high proton density in tissues (because they have a significant water component), only 20% of the lungs are made up of blood or other tissues and the rest is mostly air, thus other modalities must be used to increase the lung signal intensity.

Therefore, studies have focused on the use of hyperpolarized gas as a contrast agent, in particular, ^{3}He and ^{129}Xe. They are two noble gas isotopes, stables, non-radioactive and with a 1/2 nuclear spin.

1.3.1. ^{3}He and ^{129}Xe Advantages and Limitations

The first HP gas MRI studies were conducted in 1994 using the isotope ^{129}Xe, but because the signal intensity was restricted by the low polarization that could be achieved using the

techniques at the time (1-2%), interest in ^{3}He imaging quickly gained popularity. Some of its advantages include a larger achievable polarization (30%), a larger gyromagnetic ratio and it does not show any physiological side effects while ^{129}Xe is known to have anesthetic qualities.

Nevertheless, ^{3}He is a product of the decay of Tritium, a key component in nuclear weapons with a half-life of 12 years and after the September 11 terrorist attacks, the United States' stockpile of helium-3 has been significantly reduced as a result of the war on terror that followed. This is because Helium-3 is used in neutron detectors at our ports and borders to find hidden nuclear materials. Furthermore, its price is quickly going up, and to overcome these limitations in recent years ^{129}Xe has been reintroduced for MR imaging.

Furthermore, unlike Helium-3, Xenon-129 can diffuse into the lung parenchyma and bloodstream through the process of pulmonary gas exchange just like Oxygen and Nitrogen. Finally the most important property of ^{129}Xe is that it possesses a distinct chemical shift (change in spin frequency) between the gas phase and the dissolved phase in the lung parenchyma and another distinct chemical shift when dissolved and diffused into red blood cells. For this reason, MR researchers have shifted their interest from Helium to Xenon imaging.

1.4.   Preclinical Studies

Given the growing field of research in hyperpolarized gas imaging techniques, the need for additional preclinical studies becomes apparent. These studies are vital in providing valuable insights into human diseases and health conditions by utilizing appropriate experimental animal models. Animal models serve as a crucial bridge, connecting initial laboratory discoveries with direct testing on humans in clinical settings.

While previous studies in small animal hyperpolarized gas magnetic resonance imaging (MRI) have predominantly concentrated on rabbits, guinea pigs, and rats, there is a critical need to expand the application of this imaging modality to include mice. Mice occupy a prominent position in biomedical research due to their genetic similarities to humans and their widespread use in various experimental studies. Including mice as animal models for hyperpolarized gas MRI allows for a more comprehensive understanding of lung physiology and pathology, thereby facilitating translation to human applications.

1.4.1.   Similarity between the Respiratory System of Humans and Mice

In recent decades, mice and rats have emerged as a main pillar of contemporary biomedical research thanks due to several benefits this species is thought to offer: a well-characterized genome, a short reproductive cycle, a well-understood immunologic system, and low cost of maintenance [3]. Furthermore, there exist several noteworthy similarities between the respiratory systems of humans and mice. Firstly, both species share a comparable basic anatomical structure of the respiratory system. This includes the presence of essential components such as the nasal cavity, pharynx, larynx, trachea, bronchi, and lungs. The lung structure itself exhibits similarities, with both humans and mice possessing alveoli, the tiny air sacs responsible for gas exchange.

Secondly, the breathing mechanism employed by both mice and humans is fundamentally alike. In both cases, the contraction and relaxation of muscles within the chest and diaphragm contribute to alterations in air pressure, facilitating the inhalation and exhalation of air into and out of the lungs. This shared physiological process underscores the comparable respiratory dynamics observed in humans and mice.

Moreover, the immune response within the respiratory system also exhibits parallels between these two species. Both humans and mice possess a similar population of immune cells within the lung, including macrophages, neutrophils, and lymphocytes. These immune cells play crucial roles in defending against pathogens and maintaining the overall health and functioning of the respiratory system. The presence of comparable immune cell populations further highlights the translational relevance and significance of utilizing mice as animal models in respiratory research.

In summary, the similarities in anatomical structure, breathing mechanisms, and immune responses between humans and mice underscore the importance of extending hyperpolarized gas magnetic resonance imaging (MRI) studies to include mice. By leveraging these similarities, researchers can gain valuable insights into the respiratory system's functionality and pathophysiology, ultimately contributing to advancements in the diagnosis, treatment, and understanding of respiratory diseases in both human and mouse populations.

1.4.2.   Anesthesia

During Magnetic Resonance Imaging (MRI) procedures involving rats, the administration of anesthesia is a crucial aspect. Typically, either inhaled or injectable anesthetics are

employed for this purpose.

In the case of inhaled anesthetics, a nose cone or inhalation system is utilized to deliver a controlled mixture of anesthetic gas and oxygen. This approach is preferred due to its ability to precisely regulate anesthesia levels and easily adjust the concentration of the anesthetic based on the specific requirements of the patient. Moreover, inhaled anesthetics offer the advantage of swift discontinuation if needed, enabling prompt recovery from anesthesia.

Alternatively, injectable anesthetics can be administered through various routes, including intraperitoneal (into the abdominal cavity), intramuscular, or intravenous injection. Injectable anesthetics can induce deeper sedation compared to inhaled anesthetics but necessitate careful attention to prevent over- or under-dosing.

1.4.3. Limited Application of Animal Models in MRI Studies

Nevertheless, hyperpolarized gas MRI animal studies have only seen limited application. This is partially due to the fact that HP gas MRI is easier to perform on human subjects because they can inhale and hold their breath as opposed to uncooperative animals that need to be anesthetized and ventilated [16]. Other challenges regard the small size of the animal and the need for specialized equipment. The small size of the mouse lung limits the amount of hyperpolarized gas that can be delivered to the lung, resulting in difficulties to obtain high-quality images. This requires specialized MRI coils and specialized delivery systems that are designed for small animals.

Secondly, the mouse's respiratory rate is high, which can make it difficult to capture images during the breathing cycle. This requires the use of specialized gating techniques that synchronize the image acquisition with the breathing cycle, to minimize motion artifacts.

The choice of anesthetic depends on several factors, including the individual needs of the animal, the patient's condition, and the duration of the MRI examination. Commonly employed inhaled anesthetics for rats encompass isoflurane, sevoflurane, or desflurane. Injectable anesthetics, such as ketamine or xylazine, may be utilized in combination with an inhaled anesthetic to achieve a deeper level of sedation when required.

Within the preclinical MRI facility at the University of Illinois, a notable approach is taken to integrate anesthesia with the oxygen supply. This integration enables extended testing periods while simultaneously reducing invasiveness for the animals. By seamlessly incorporating anesthesia with the oxygen supply, the facility ensures optimal conditions

for conducting comprehensive MRI examinations on rats.

1.4.4. Hyperpolarized Gas Delivery in Small Animals

In vivo imaging tests conducted on sedated rabbits [12] have demonstrated that the simplest method for administering hyperpolarized (HP) ^{129}Xe to animals is by administering a single bolus using a gas syringe. This technique offers precise control over the administered volume, allowing for accurate delivery of hyperpolarized xenon gas. Additionally, it enables imaging to be performed even during suspended lung motion, providing valuable insights into lung dynamics. However, a limitation of this approach is related to the small volume of hyperpolarized Xenon gas that can be administered. As a result, the achievable spatial resolution is inherently restricted to a single 2D slice.

The aforementioned limitation becomes particularly pronounced when working with rats and mice due to their smaller tidal volumes (0.2 ml for mice and 2 ml for rats) and the higher spatial resolution requirements associated with imaging in these smaller subjects. To address this challenge, it is necessary to administer multiple tidal volumes of hyperpolarized gas in order to generate an adequate level of magnetization for high-resolution magnetic resonance imaging (MRI) in rodents. Additionally, image data needs to be acquired over multiple breathing cycles to gather sufficient information.

For the reasons mentioned in the last subsection, the application of HP ^{129}Xe MRI and MRE in small animal models, in particular, poses unique technical challenges. To summarize:

- It requires precise external control of the quantity and timing of HP gas alternating with anesthesia delivery to the breathing animal.

- The experiment must be fully instrumented and carried out using materials that are allowed in ultra-high field MRIs that do not cause HP gas depolarization and do not degrade image acquisition.

One solution that was proposed to overcome these limitations was to deliver the hyperpolarized gas continuously to spontaneously breathing, anesthetized mice [9]. However, this approach was found to be affected by irregular breathing patterns of varying depths that could cause motion artifacts or limit the resolution of the images obtained. In other words, continuous delivery of hyperpolarized gas could result in inconsistent gas exchange and distribution in the lungs, which could affect the quality of the captured images. This is because mice have a high respiratory rate and their breathing depth can vary.

As a result, different methods have since been developed to enhance the procedure. A

better solution involves the use of mechanical ventilation to control the animal's respiration via positive pressure. By using this method, the respiratory motion of the mouse can be suspended, allowing for improved imaging quality and resolution. This is achieved by performing full three-dimensional encoding of the lungs incrementally over multiple breathing cycles, which ensures complete coverage of the lung volume and reduces the risk of motion artifacts. The use of mechanical ventilation allows for precise control of the mouse's breathing rate and depth, which minimizes the variability in gas exchange and distribution within the lungs. Gating the imaging acquisition to the respiratory cycle further improves the quality of the images obtained by ensuring consistency during the breathing cycle.

Overall, this method is a more effective approach to performing hyperpolarized gas MRI in mice, providing improved image quality and reliable measurements of lung function.

1.5.   Project Aim

The primary objective of this project is to develop a portable hyperpolarized (HP) gas ventilator capable of facilitating high-resolution three-dimensional (3D) imaging of dissolved and gas-phase ^{129}Xe in the lungs. The envisioned device is specifically designed to be compatible with the 9.4 Tesla preclinical MRI system within the UIC RRC Preclinical Imaging Core (Figure 1.1).

Figure 1.1: 9.4 Tesla preclinical MRI system within the UIC RRC Preclinical Imaging Core.

Addressing the aforementioned challenge of achieving precise control over very small tidal volumes required for mice, the developed ventilator incorporates differential pressure transducers and a 3D-printed pneumotachometer. These components ensure accurate measurement of tidal volume and enable precise control over breathing cycles, effectively

overcoming this limitation. Furthermore, a notable benefit of this ventilator is its affordability and reproducibility. The utilization of low-cost microcontrollers, 3D printed parts, and the implementation of a system to recapture expelled high-pressure gases significantly reduce the overall cost per study. This affordability not only makes the device more accessible but also promotes its broader adoption in preclinical research settings.

In addition to its cost-effectiveness, the ventilator offers the advantage of adaptability. It is designed to accommodate various small animal models such as rats, mice, guinea pigs, and rabbits. By providing this versatility, the ventilator facilitates experiments involving different animal species, allowing for comparative studies and expanding the potential applications of the device. Moreover, the ventilator eliminates the need for tracheotomy, a surgical procedure often required in animal studies, thereby enhancing the post-study survivability of the animal participants and minimizing potential complications associated with invasive procedures. The subsequent chapter in the thesis will provide a detailed outline of the step-by-step process necessary to achieve the outlined objectives. This chapter will guide the reader through the various stages of the project, providing comprehensive instructions and explanations to ensure a thorough understanding of the development and implementation of the ventilator.

2 | Ventilator Development

Chapter 3 of this thesis provides an extensive and comprehensive account of the implementation of the ventilator. The chapter is structured as follows:

Section 3.1 begins with a comprehensive review of the requirements that the ventilator must meet. This section serves as a reminder of the critical aspects that guided the development process, ensuring that the ventilator fulfills the necessary criteria.

Following that, Section 3.2 provides a concise summary of the ventilator's functioning and its overall architecture. It offers an overview of the key operating principles and highlights the core components of the system.

In Section 3.3, a detailed breakdown of the components utilized in the ventilator is presented, along with their specific characteristics. This thorough examination ensures a comprehensive understanding of the materials and devices employed in the implementation.

Section 3.4 is dedicated to discussing the Pneumotachometer, a vital feature of the ventilator that enables precise control over tidal volume. This section not only explains the fundamental concepts and principles behind the Pneumotachometer but also delves into the calibration process undertaken to ensure its accuracy and reliability.

Moving forward, Section 3.5 focuses on the hardware aspects of the ventilator. It elaborates on the various electronic connections and circuitry that enable the smooth operation of the device. Detailed descriptions of the hardware components and their interconnections are provided, ensuring a comprehensive understanding of the system's physical configuration.

In Section 3.6, the coding aspects of the ventilator are discussed in detail. This section encompasses the firmware development in the Arduino IDE, which controls critical functions such as valve activation and mode switching. Furthermore, the user interface, allowing real-time monitoring of data, is presented, underscoring the importance of user-friendly and accessible interfaces in enhancing usability.

By organizing the chapter in this manner, readers are provided with a thorough understanding of the ventilator implementation. The section-wise breakdown ensures that each aspect of the ventilator, from requirements to hardware and coding, is comprehensively addressed, allowing for a holistic view of the development process.

It is pertinent to emphasize that the development of the device builds upon the design initially presented by Nouls et al. in 2011 [16], and subsequently in 2018 [20]. This thesis introduces the pneumotachometer as a novel method for controlling tidal volume in ventilation, offering a departure from the existing state of the art. The developed device incorporates this innovation, providing precise and accurate volume regulation. Additionally, the thesis highlights the original development of ventilator control codes and the user interface from scratch, allowing for tailored customization and effective user interaction. These contributions bring unique value to the research field and enhance advanced ventilation monitoring and control possibilities.

2.1.   Ventilator Requirements

To recap, the ventilator must be compatible with the 9.4 Tesla preclinical MRI system within the UIC RRC Preclinical Imaging Core and it has to avoid HP gas depolarization. To meet these significant requirements important elements must be considered when developing the device:

- Paramagnetic oxygen and HP gas must be mixed as late as possible in the gas delivery process since oxygen can depolarize the Xenon.

- HP gas must be handled using only materials that contain no ferrous impurities.

- To prevent any interference with the magnetic field of the MRI scanner all parts of the ventilator must be made of non-magnetic materials, such as aluminum, brass, or plastic.

- The ventilator must have motors and electronics that are shielded. This is typically achieved through the use of copper shielding or other materials that can block electromagnetic interference.

- It must deliver the same tidal volume and precisely position the lung throughout each cycle in order to collect image data over several breaths.

- The ventilator should be easy to use, with simple controls that can be operated by a technician or a research student. It should also be easy to move in and out of the MRI room.

2.2.   Ventilator Architecture

The system comprises two sections: an MR-compatible mechanical part and a non-MR-compatible electronic module.

2.2.1.   Electronic Module

The electronic module serves as the primary user interface, allowing for the modification of the breathing pattern and continuous monitoring of pressures and tidal volume. More specifically, this module encompasses the power supplies and incorporates two separate microcontrollers: a Raspberry Pi and an Arduino. The Raspberry Pi is a single-board computer with a Linux operating system. It is connected to a keyboard and a monitor to present the user interface, enabling the adjustment and control of various parameters.

However, the Raspberry Pi is not suitable for precise timing control due to potential interruptions by its operating system. To address this, an Arduino microcontroller is employed. The Arduino operates without an operating system and is capable of reliably generating precisely timed signals for valve actuation. Additionally, it can trigger MR data acquisition at the desired phase of the respiratory cycle. The Arduino functions independently, complementing the Raspberry Pi's limitations and fulfilling the task of precise timing control.

2.2.2.   Mechanical Module

The mechanical part administers the appropriate gas mixture (O_2 plus Anesthesia, N_2, and HP gas), regulates breath-hold, and permits passive exhalation utilizing fast-actuating solenoid or pneumatic valves. The ventilator delivers a mixture of 75% N_2 and 25% O_2 during normal breathing, and it is made to replace nitrogen with HP gas during HP gas MRI/MRE. Figure 2.1 shows the ventilator design:

On the right side, there are the Oxygen line (already integrated with isoflurane for anesthesia) and the Nitrogen line, while on the left there is the animal trachea. Their pressures are controlled by regulators and also checked by analog pressure sensors.

During normal breathing, the delivery of these two gasses is controlled by solenoid valves, while when there is the need to ventilate the animal with the HP gas, the line of nitrogen is turned off. The administration of HP gas is controlled by using a pneumatic valve made entirely of fluoropolymer, as opposed to the fast-switching metal solenoid valves that control the delivery of nitrogen and oxygen. A solenoid valve is used to open and
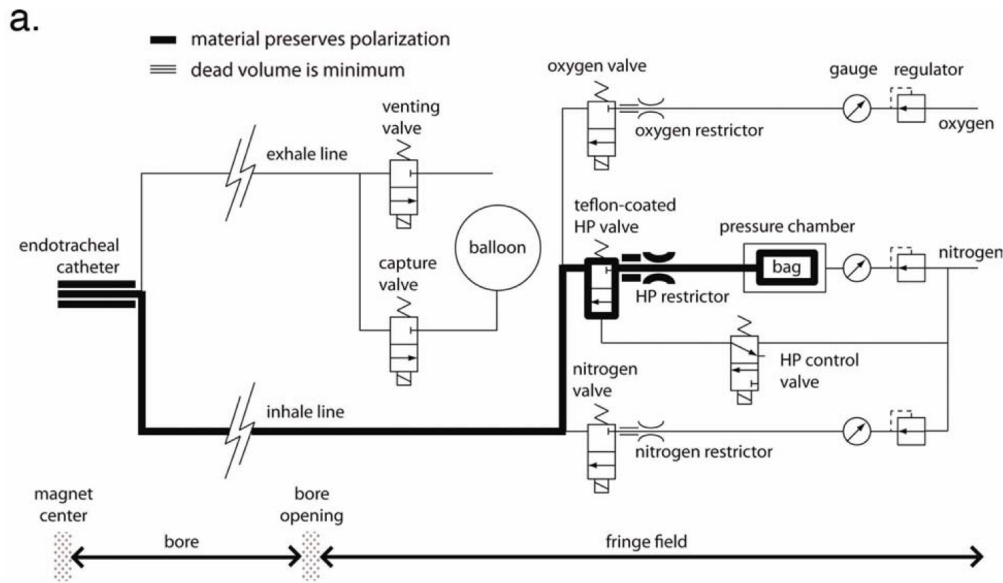
Figure 2.1: Schematic of the ventilator presented by Nouls et al. in 2011.

close this pneumatic valve in response to pressure variations.

The delivery of hyperpolarized (HP) gas involves a Tedlar bag located within a rigid chamber that is pressurized by nitrogen (N_2). To ensure the preservation of HP gas polarization, oxygen and either xenon or nitrogen are kept separate for as long as possible. They are combined in the trachea of the animal to prevent depolarization of the HP gas. On the exhale line, a pneumotachometer will be used to monitor the tidal volume and there will be the option to expel the gas into the atmosphere or recapture the gas into a balloon for further reuse.

All the components will be explained in detail in the following chapters.

2.3. Physical Implementations

2.3.1. Nitrogen and Oxygen Line

The initial element that the gas encounters in the ventilator system is the regulator, specifically the R7010 AirLogic model manufactured by Racine, WI, (Figure 2.2).

The Precision Pressure Regulator is an essential component designed to regulate the pressure within the system. It is capable of receiving input pressures ranging from 0 to 150 PSI, while providing precise output pressures within the range of 0 to 10 PSI.

Figure 2.2: Regulator: R7010 AirLogic, Racine, WI.

The regulator is equipped with an input door, an output door, and two blank ports as standard features. What sets this regulator apart is its construction using materials such as Stainless Steel, PVC, Carbon, and Glass, which make it resilient to the high magnetic field of MRI environments. This ensures the regulator performs reliably and maintains accurate pressure control within the system. In the design of the ventilator, three regulators are incorporated: one in the oxygen line and two in the nitrogen line. The former in the nitrogen line is responsible for controlling the pressure within the pressure chamber tube, while the latter regulates the nitrogen pressure during normal operation. These regulators play a crucial role in maintaining the desired pressure levels within the system, ensuring optimal performance and safety.

To verify and monitor the pressure levels accurately, analog pressure transducers are utilized. Specifically, the project utilizes the Fujikura Pressure Sensors, AG2 model (Figure 2.3). These pressure sensors consist of a silicon piezoresistive pressure sensing chip and a signal conditioning integrated circuit. The pressure-sensing chip within the sensor converts the low-level pressure signal into a high-level output signal that is directly proportional to the applied pressure. In this project, three sensors with a range of 50KPa are employed, with each sensor dedicated to monitoring the pressure on a specific line. These sensors provide accurate and reliable pressure measurements, ensuring precise control and monitoring of the system.

These sensors incorporate advanced technology, offering high performance, reliability, and durability. Fujikura has integrated signal processing and compensation algorithms into the AG2 series, aiming to minimize signal distortions and variations caused by temperature fluctuations. This feature is intended to ensure that pressure readings remain reliable and accurate under different environmental conditions.

Figure 2.3: Fujikura Pressure Sensors, AG2 Series.

The combination of the precision pressure regulators and the Fujikura pressure sensors in the ventilator system ensures effective pressure control, accurate monitoring, and reliable operation. Within this particular project, pressure sensors with a range of 50KPa have been specifically chosen for implementation. This range is well-suited for the intended applications and requirements of the ventilator system, allowing for precise measurement and control of the pressure within the system.

At this stage of the project, the control of Nitrogen and Oxygen delivery is achieved through the utilization of fast-switching solenoid valves, specifically the EC-2-12-H model by Clippard (Cincinnati, OH), Figure 2.4. During normal breathing, these valves regulate the flow of Nitrogen and Oxygen. However, during HP (hyperpolarized) ventilation, the Nitrogen valve is deactivated, and an additional solenoid valve, identical to the ones controlling the Nitrogen and Oxygen lines, is activated to manage the Teflon valve responsible for the release of HP gas.

In total, four fast-switching solenoid valves are employed in this project. One valve is dedicated to the Oxygen line, another to the Nitrogen gas line, a third valve is situated in the exhale line, and the last valve is utilized to control the delivery of HP gas. The Clippard EV series valves are chosen solenoid valves known for their quiet operation and low-power design. They feature a simple configuration with the primary moving component being the Clippard "spider" armature spring, requiring minimal displacement of 0.007 inches for valve opening. These valves have been tested and proven to have an impressive lifespan exceeding 1 billion cycles, demonstrating their durability. Actuated by low-voltage DC inputs, they offer rapid response times ranging from 5 to 10 milliseconds while consuming only 0.67 watts of power. Additionally, the EV series valves operate quietly and their lightweight, compact design allows for easy installation in confined spaces.

Figure 2.4: Solenoid valve model EC-2-12-H, Clippard, Cincinnati, OH.

2.3.2. Hyperpolarized ^{129}Xe Line

The extraction of Xenon gas, comprising approximately 26% of the isotope ^{129}Xe, was carried out utilizing the Polarean 9820 hyperpolarizer (Figure 2.5).

Figure 2.5: Polarean 9820 Hyperpolarizer.

This hyperpolarization process involved the extraction of Xenon from a mixture of various gases, including Nitrogen and Helium. Following the completion of the extraction process, the hyperpolarized Xenon gas was stored within a Tedlar bag hyperpolarized, Figure 2.6. While the detailed explanation of the hyperpolarization process is omitted in this thesis due to the absence of testing the ventilator with the hyperpolarized gas, it is essential to acknowledge the source of the hyperpolarized Xenon.

Once the hyperpolarized (HP) Xenon gas has been successfully collected and stored in the Tedlar bag, the subsequent step involves placing the bag within a chamber. This chamber is specifically designed to accommodate the Tedlar bag and serves the purpose of pressurizing the enclosed gas. Notably, the pressurization of the chamber is achieved through
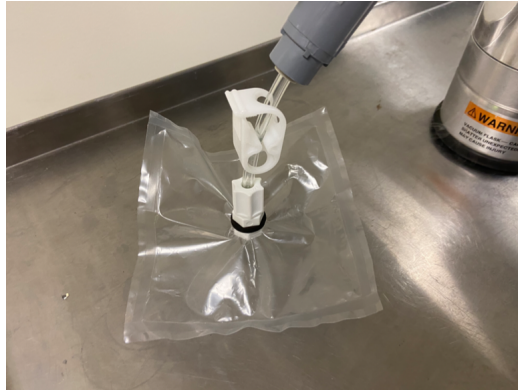
Figure 2.6: Vacuumed Tedlar bag, where hyperpolarized Xenon from Polarean 9820 polarizer is stored.

the introduction of Nitrogen gas (N2), which creates the necessary pressure environment for the hyperpolarized Xenon gas to be utilized effectively within the experimental setup, Figure 2.7.
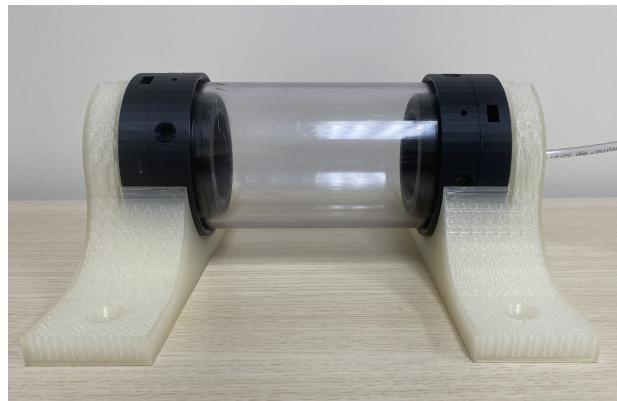
Figure 2.7: Pressure Chamber, where Hyperpolarized Xenon is placed during ventilation.

All the components depicted in the provided image have been meticulously constructed using Solidworks.

First and foremost, the tube pressure holders, a noteworthy addition to our design, have been fabricated through 3D printing techniques utilizing PLA (Polylactic Acid) as the selected material. PLA was chosen due to its affordability and inherent rigidity, both of which are crucial factors in the effective functioning of pressure holders. In addition to their primary function of securely holding the pressure chamber, the tube pressure holders serve an additional purpose by providing an added layer of safety. By being firmly attached to the ventilator box using screws, they effectively prevent the expansion of the chamber in the event of joint failure or an occurrence of extremely high pressure. This safety feature acts as a safeguard against potential accidents or hazards that may
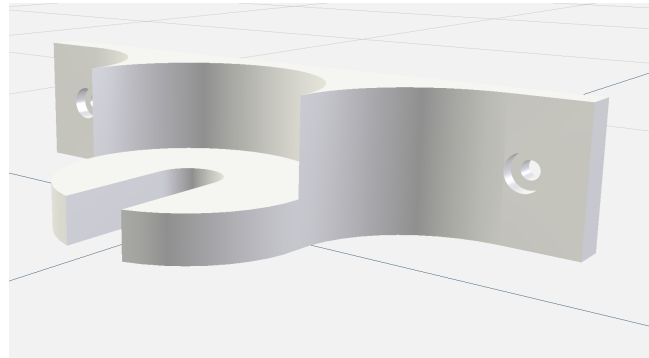
Figure 2.8: Brackets that hold the pressure chamber in STL format.
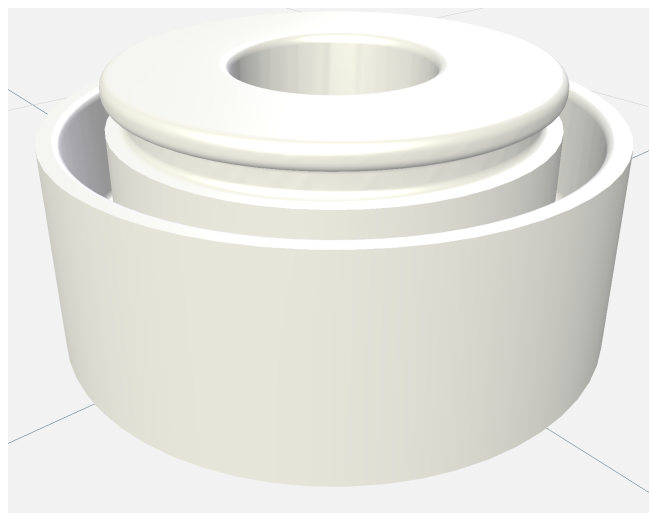
Figure 2.9: Pressure chamber junction, side view.

arise from such situations, Figure 2.8.

This component is not present in the ventilator developed by Nouls et. al so so it represents a new feature in our design. Furthermore, the image showcases the junctions specifically designed to maintain the pressurization of the vessel. Although inspired by the design concept employed in Nouls' ventilator, certain modifications have been implemented in terms of the geometric configuration. These alterations have been made with the intention of improving upon the existing design and ensuring optimal performance in our ventilator (Figure 2.9).

The development of the ventilator presented a significant challenge, as one of the primary objectives was to devise a solution that effectively maintained chamber pressurization and minimized air leakage. This task demanded considerable effort and time to identify an optimal approach.

Initially, the components crucial to the pressurization mechanism were fabricated using

3D printing technology and Polylactic Acid (PLA) as the chosen material. However, it became apparent that PLA exhibited inherent limitations, such as high porosity and permeability to water. Consequently, a series of innovative strategies were explored in order to address these issues.

The first attempt involved applying a waterproof spray treatment to the PLA components. Despite this initial intervention, air leakages persisted. Recognizing the need for an alternative approach, attention was turned towards simplifying the geometry of the junctions in an effort to enhance the printing process and eliminate potential porous spaces. However, this modification alone did not yield the desired solution to the problem at hand.

Ultimately, a decision was made to employ a different material for printing the simplified geometry of the junctions, leading to the selection of a resin material. It is important to note that this choice incurred additional expenses, with each piece costing approximately $85. However, the implementation of this alternative material resulted in a significant reduction in air leakage. To substantiate this improvement, a validation test was conducted. The pressure chamber, in conjunction with the junctions, was submerged in water while air was continuously flowing through the system. Observations revealed the absence of air bubbles, thereby affirming the effectiveness of the chosen material in preventing air leakage.

Moreover, to ensure a robust and secure connection within the tubes, rubber gaskets were utilized to maintain and seal the junctions. This additional measure further enhanced the integrity of the system and minimized the risk of any potential air leakage.

From the pressure vessel, the ^{129}Xe delivery is controlled by using a pneumatic valve made entirely of fluoropolymer (model PV-1-1134, Partek Division, Parker Hannifin, Tucson, AZ, Figure 2.10). The PV-1 Series is made for applications involving semiconductors, ultra-pure water, and potent chemicals or gases. The body, seat, and diaphragm of the design are made of machined modified PTFE, which ensures outstanding flexibility and long life. During the ventilation process with hyperpolarized gas, the Nitrogen solenoid valve is closed and the pneumatic valve is opened and closed by pressure changes controlled by a third solenoid valve identical to those governing the N2 and O2 lines.

As illustrated in Figure 2.1, the functioning of the hyperpolarized (HP) gas line exhibits slight variations compared to the oxygen and nitrogen lines. These distinctions arise from the distinctive properties associated with hyperpolarized gas. Specifically, HP gas cannot pass through a conventional metallic solenoid valve without experiencing significant depolarization. To address this limitation, the schematic indicates the sections of the

Figure 2.10: Pneumatic, fluoropolymer valve, model PV-1-1134, Partek Division, Parker Hannifin, Tucson, AZ.
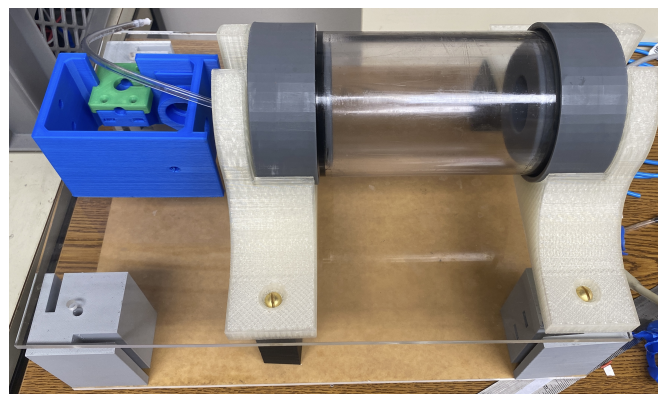

Figure 2.11: Ventilator Box.

ventilator where nondepolarizing materials must be employed. These areas include the HP gas valve, restrictors, and inhale tubing.

In the case of the flow restrictor, the Nouls' ventilator utilizes sapphire embedded in nylon as the chosen material. For the inhale tubing, a single 1-meter-long polyether ether ketone (PEEK) line, specifically the TPK130 model from Vici Valco instruments, has been employed [16]. Furthermore, Oxygen is a source of depolarization, thus the two lines are not combined until they reach the mouthpiece. This prevents contact from occurring during the 140-ms inspiration period and results in a 1.6% oxygen-induced depolarization. All the aforementioned components, including the gas-delivery valves, pressure transducers, and the HP gas supply, are housed within the ventilator box (Figure 2.11).

This structure comprises a total of six columns, with four relatively larger columns posi-
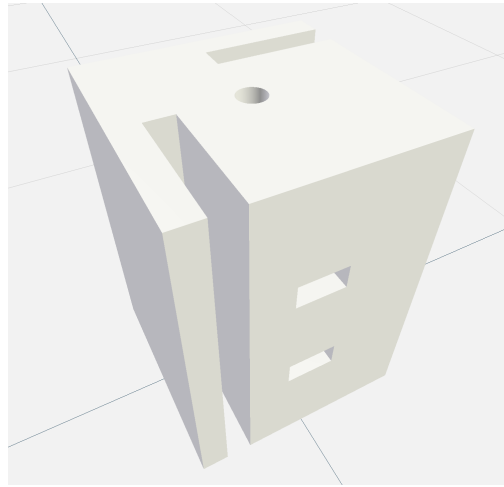
Figure 2.12: Corner column equipped with a side slot, intended for the attachment of a side facade, and it is constructed using 3D printing technology with PLA material.

tioned at the corners of the box, and two comparatively narrower columns situated in the middle, that serve as the pressure chamber's engagement points. Notably, these columns were designed using Solidworks, a popular computer-aided design (CAD) software, and subsequently fabricated using a 3D printer, employing PLA (Polylactic Acid) as the printing material. Upon careful examination of the Solidworks model (Figure 2.12), it becomes apparent that the thicker columns incorporate a slot on its side, specifically intended to accommodate the attachment of a side facade, instead the top and bottom facades are actually affixed to the structure through the use of brass screws.

Furthermore, it is worth mentioning that all the facades were produced using laser cutting techniques, which involve the use of laser technology to precisely cut and shape the desired materials. This method offers a high level of accuracy and ensures clean and precise edges for the resulting facades.

2.3.3.   Exhale Line

The conclusion of the inspiration phase is marked by the closure of valves responsible for regulating the flow of oxygen, nitrogen, or hyperpolarized (HP) gas. This closure initiates a brief breath-hold period, which is commonly employed for the acquisition of imaging data. Subsequently, the solenoid valve that governs expiration is opened to initiate passive exhalation, enabling the lungs to return to their functional residual capacity.

During the exhalation process, the exhaled gases pass through polyether ether ketone (PEEK) tubing with an inner diameter of 1/32 inch. This PEEK tubing is specifically chosen for its low impedance, ensuring that complete exhalation occurs after each breath.
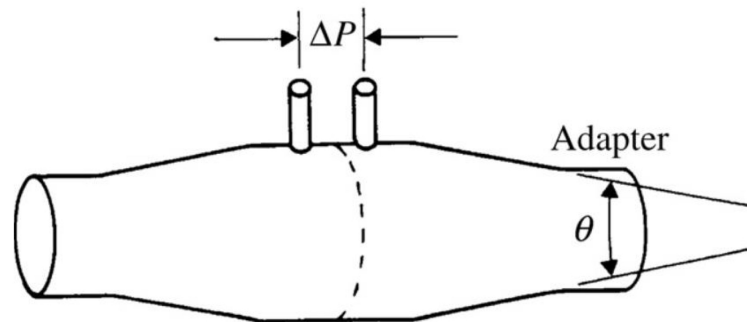
Figure 2.13: Pneumotachometer (PNT): devices that employ flow resistors that exhibit nearly linear pressure-flow relationships.

It provides an efficient pathway for the exhaled gases to exit the system. Throughout the entire breathing cycle, the tidal volume, which represents the volume of air inspired or expired during each breath, is carefully monitored using a Pneumotachometer. This component holds significant importance in the thesis work and will be comprehensively explained in the forthcoming chapter, elucidating its operation and role in the research.

During hyperpolarized (HP) gas imaging, the process of exhalation is controlled by a separate expiration valve, distinct from the one employed during normal nitrogen/oxygen breathing. This specialized valve directs the exhaled mixture of ^{3}He or ^{129}Xe to a capture balloon constructed from metalized mylar. By utilizing this distinct exhale valve, the balloon solely captures the exhaled ^{3}He or ^{129}Xe (along with residual breathing gases), minimizing dilution with ambient air that would otherwise occur during normal breathing. This deliberate separation ensures the preservation of the captured gas, allowing for its reuse in subsequent preclinical HP gas studies.

2.4.   Pneumotachometer (PNT)

Flow sensors utilized in respiratory laboratories, commonly known as pneumotachometers (Figure 2.13), have played an integral role historically and continue to be relied upon in the field. These devices employ flow resistors that exhibit nearly linear pressure-flow relationships, thereby providing accurate measurements. The term "pneumotachometer" is often used interchangeably with "gas volume flowmeter" to describe these instruments.

Pneumotachometers offer several advantageous features. They are user-friendly, allow for straightforward operation, and possess the ability to detect and differentiate the directions of alternating flows. Furthermore, these sensors exhibit a commendable level of accuracy,
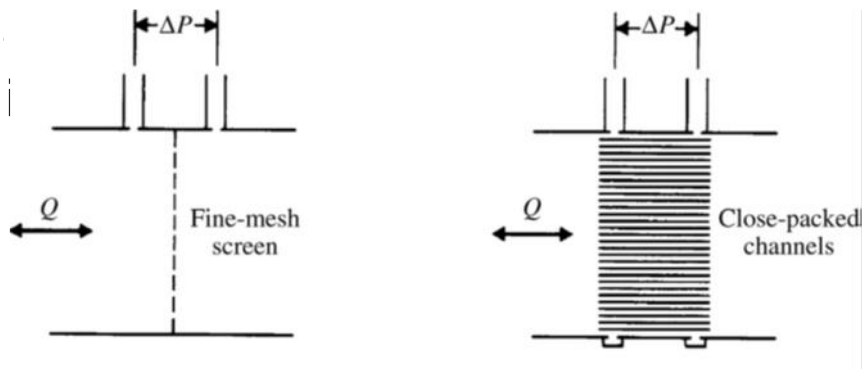
Figure 2.14: At left one PNT with fine mesh screens placed perpendicular to the flow. At the right there is a PNT with a packed bundle of capillary tubes with its axis parallel to flow.

sensitivity, linearity, and frequency response, rendering them suitable for a wide range of clinical applications. Notably, they leverage the same differential pressure sensors and amplifiers that are utilized for other respiratory measurements, contributing to their versatility and compatibility within respiratory assessment setups.

In the realm of pneumo-tachometry, while various flow-resistance elements have been integrated, it is noteworthy that the prevalent choices encompass either one or multiple delicately woven mesh screens positioned orthogonal to the flow, or a compactly arranged assemblage of capillary tubes or channels, aligned parallel to the course of flow (Fleisch), Figure 2.14. These tangible mechanisms demonstrate, over a considerable spectrum of fluctuating flows, an almost linear correspondence between pressure drop and flow, with the pressure drop exhibiting approximate synchrony with the flow.

The measurement of pressure drop at a specific radial distance from the conduit's center implies the assumption that this pressure drop effectively represents the overall pressure drop governing the total flow across the entire cross-section of the conduit. Consequently, these flowmeters rely on the presence of a flow-resistive component to establish a reasonably consistent velocity distribution on either side of the component near the pressure measurement location, albeit not achieving perfect uniformity. However, the ability to achieve this desired velocity distribution is contingent upon the specific configuration of the ductwork where the pneumotachometer is positioned. Consequently, the placement of pressure ports and the configuration of the tubing that connects the subject to the pneumotachometer, as well as the subsequent connection from the pneumotachometer to the rest of the system, play a critical role in determining the relationship between pressure drop and flow. This significance is particularly pronounced when dealing with alternating
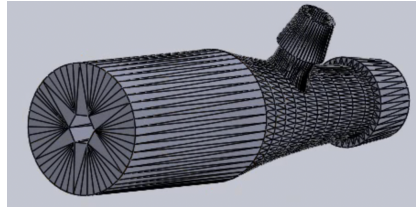
Figure 2.15: The Solidworks model of the pneumotachometer (PNT) includes detailed representations of its internal diameter and a distinctive protuberance designed for attaching the sensor.
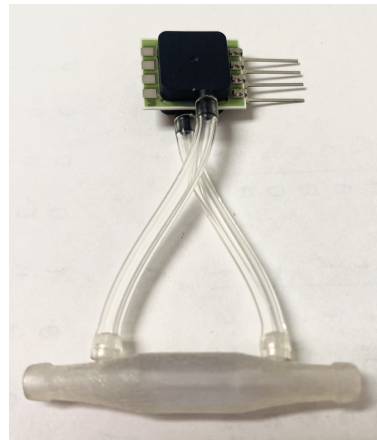

Figure 2.16: PNT with the differential pressure transducer from ELVR series.

and/or high-frequency flow patterns.

In the context of this thesis project, a deliberate decision has been made to position the pneumotachometer (PNT) at the expiration line, aiming to minimize the presence of dead volume. To facilitate this implementation, the TechRes lab graciously provided us with the Solidworks model of two PNT variants (Figure 2.15). Subsequently, we utilized 3D printing technology using VeroClear material to fabricate the physical PNT prototypes.

In order to measure the pressure across the pneumotachometer (PNT), a differential pressure sensor has been employed, Figure 2.16. This sensor is from the ELVR series and it serves the purpose of accurately detecting and quantifying the pressure difference across the PNT. By utilizing such a sensor, precise and reliable measurements of the pressure drop can be obtained, enabling an accurate assessment of the flow rate passing through the PNT. The ELVR Series Amplified Low-Pressure Sensors are highly accurate and reliable instruments designed specifically for measuring low pressures. They feature a wide input range and provide amplified output signals, simplifying integration into measurement systems. They are robust and equipped with protective features for durability in challenging environments.

In this project, we have chosen an analog sensor that operates on a 5-volt power supply and provides an analog output. This decision allows us to easily integrate the sensor into our measurement system, utilizing the analog voltage values generated by the sensor to obtain precise measurements of the variables of interest.

2.4.1.   Calibration

Calibrating the sensor is crucial for ensuring the accuracy, reliability, and traceability of measurements. The objective of the calibration process is to establish a quantitative linear relationship between the pressure values collected by the differential pressure transducer and the corresponding flow values. This relationship is represented by the equation $y = m * x + q$, where y denotes the measured flow in L/s, x represents the input pressure values in bits, and m and q are the coefficients that determine the slope and y-intercept of the linear equation, respectively. By calibrating the system and determining the values of m and q, it becomes possible to convert the pressure readings into accurate flow measurements, enabling a comprehensive analysis of the dynamic airflow within the system.

To calibrate the instrument, a syringe with a known volume of 12.5 mL was utilized. The air of this volume was passed through the interior of the pneumotachometer (PNT), and the pressure sensor measured the resulting pressure difference across the PNT. This procedure allowed for the calibration of the instrument by establishing a reference point using the known volume of air and the corresponding pressure measurements at the PNT ends. In regard to the hardware, the establishment of a reliable connection involved the utilization of a breadboard for convenient circuit prototyping. The sensor, serving as a pivotal component, was carefully integrated with Arduino through a dedicated conditioning circuit.

In adherence to best practices and specifications, the schematic design incorporated essential elements to optimize the electrical performance. To stabilize the power supply, a 100nF capacitor was strategically placed between the ground and the power lines, ensuring a consistent and reliable voltage level. Moreover, a 10nF capacitor, in accordance with the specifications outlined in the sensor's datasheet, was implemented at the analog output. To further refine the signal, a 50 Hz low-pass filter was employed, effectively attenuating higher-frequency noise components. The design of this filter entailed the utilization of a 10Kohm resistor and a 100nF capacitor.

To maintain signal integrity and enable seamless interfacing with the Arduino's analog-to-digital converter (ADC), an operational amplifier (Opamp), model MCP6044-E/ST
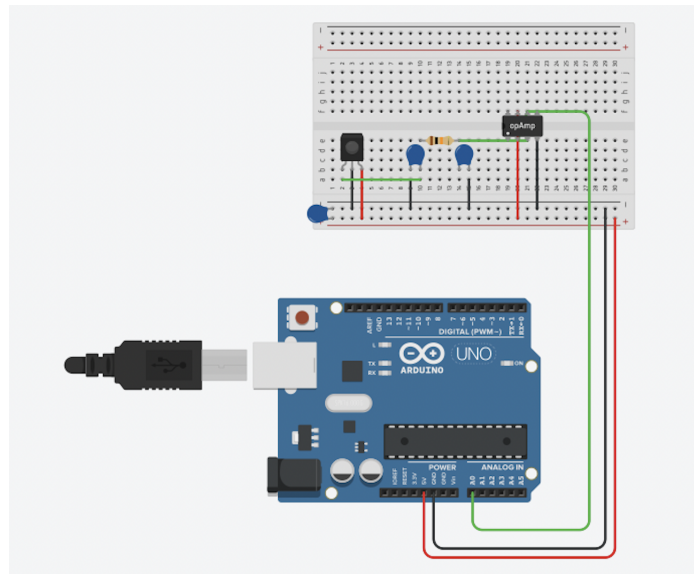
Figure 2.17: Calibration setup: Breadboard, Arduino, differential pressure sensor (connected to PIN A0), and conditioning circuit.
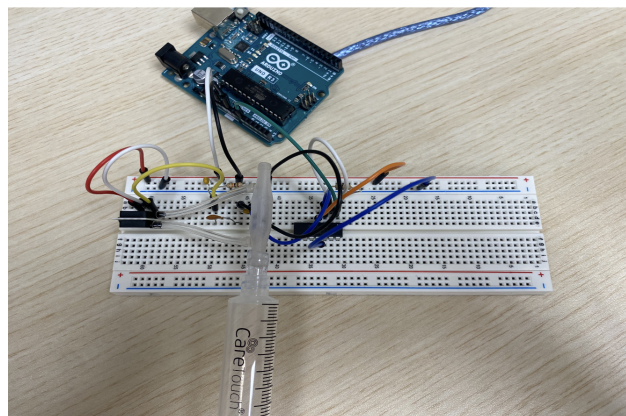

Figure 2.18: Calibration Hardware Setup.

from Microchip Technology, was incorporated. Specifically, the Opamp was configured as either a Buffer or a Voltage Follower, ensuring high input impedance and low output impedance. This configuration allowed for optimal signal transmission without compromising the integrity of the original signal, (Figures 2.17, 2.18). By diligently implementing these electronic connections and employing appropriate circuitry, the sensor's output was effectively conditioned and interfaced with the Arduino platform, facilitating accurate and reliable data acquisition and processing.

To facilitate data acquisition, a straightforward firmware was developed using the Arduino IDE. As the syringe controlled the movement of a known volume of air within the pneumotachometer (PNT), a vital aspect of the data acquisition involved the continu-

ous monitoring of the pressure differential across the PNT. To achieve this, an interrupt routine was implemented with a frequency of 250Hz. This interrupt routine enabled the real-time detection and measurement of the pressure difference between the downstream and upstream ends of the PNT.

An interrupt service routine (ISR), also known as an interrupt handler, is a specialized routine within a computer program that is designed to respond to interrupts. Interrupts are signals or events generated by hardware devices or software conditions that require immediate attention from the central processing unit (CPU). When an interrupt occurs, the CPU temporarily suspends its current execution and transfers control to the ISR. In the thesis project, the timer overflow event is utilized as the trigger for generating interrupts. This event occurs when the timer reaches its maximum value and resets to zero. With each timer overflow, an interrupt is generated. This approach ensures a consistent and stable interrupt frequency, which is ideal for sampling a signal, ensuring that data points are captured at regular intervals. Overall, utilizing the timer overflow as the interrupt source provides a robust foundation for signal sampling. It ensures that interrupts occur at predetermined and evenly spaced intervals, facilitating accurate and synchronized data acquisition.

Thus in this calibration process, the firmware and the syringe worked in parallel during data acquisition. While the syringe controlled the airflow through the PNT, the firmware executed an interrupt routine to capture pressure data. This simultaneous operation enabled real-time measurements of pressure differentials, providing accurate and continuous monitoring of the dynamic airflow within the PNT.

To assess the proper functioning of the interrupt code, a straightforward mathematical calculation was performed. Given the interrupt frequency of 250, it indicates that within a single second, 250 interrupts occur. As each interrupt corresponds to the acquisition of one data point, it implies that within one second, we would have 250 data points. To verify this, we examined whether after 10 seconds, the total number of acquired data points amounted to 2500.

In addition to the data acquisition system, a User Interface (UI) was developed using Processing to visualize the real-time data, Figure 2.19. Processing is an open-source programming language and environment specifically designed for creating interactive graphics and visualizations. It provides a user-friendly platform for artists, designers, and developers to explore visual representations of data.

The UI developed with Processing includes two buttons: a start button to initiate data acquisition and a stop button to halt the process. This allows users to easily control the
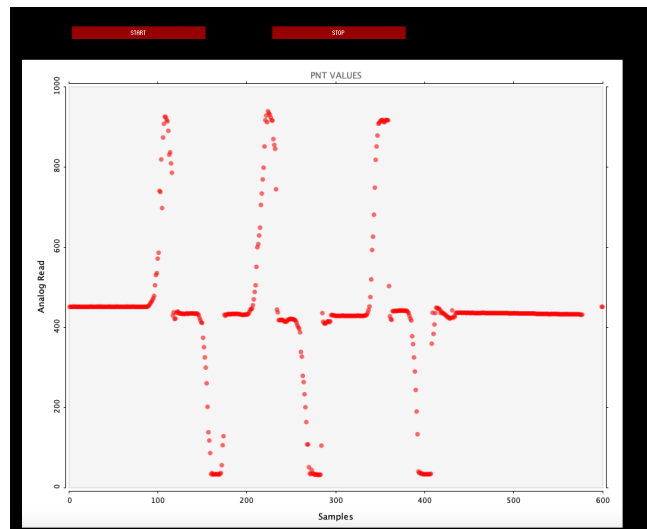
Figure 2.19: Image showing data acquisition in Processing during syringe movement. The baseline level is at 450, positive peaks represent syringe pushing, while lower peaks represent syringe pulling.

data acquisition system according to their requirements. In this case, the UI displays a graph that illustrates the data trends based on the speed of the syringe movement.

The collected data is saved to a text file, ensuring its persistence and facilitating further analysis. In fact, in this project, MATLAB has been used to assess the calibration coefficients. At this point, the recorded data stored in the designated txt file underwent comprehensive analysis using MATLAB, a powerful software tool for data processing and visualization. The recorded measurements, ranging from 0 to 1023, were initially represented as discrete values and interpreted as bit representations (Figure 2.20). The main objective of the calibration was to establish a quantitative relationship between these pressure values in bits and the corresponding flow values in L/s. This objective was achieved by taking advantage of the inherent linear relationship that exists between pressure and flow when employing the pneumotachometer.

To facilitate this conversion, it has been incorporated the CalFlow function, provided by the esteemed TechRes lab affiliated with the Politecnico di Milano. This specialized function was carefully integrated into the analytical framework, accepting a column vector containing the flow measurements requiring calibration as input.

Following the execution of the CalFlow function, the user was prompted to provide the acquisition frequency, which determined the sampling rate of the data. Subsequently, the function offered a graphical representation of the acquired data, affording the user the opportunity to accurately select the baseline point. The function then calculated the
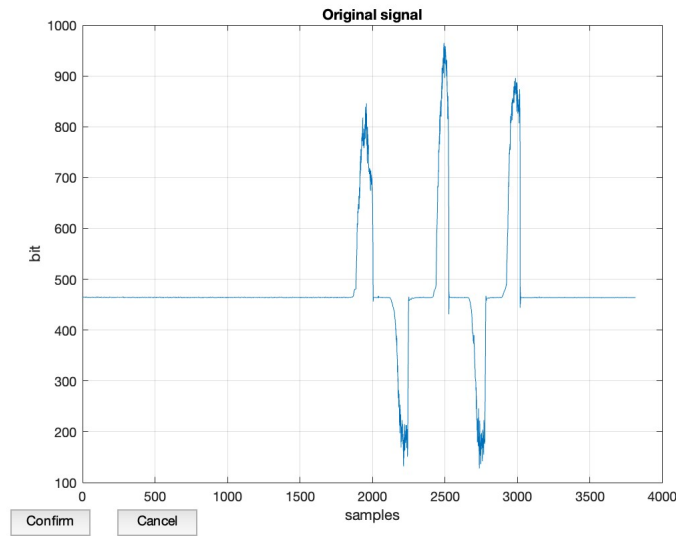
Figure 2.20: Plot of Pressure Data (in Bits) from TXT File in MATLAB.
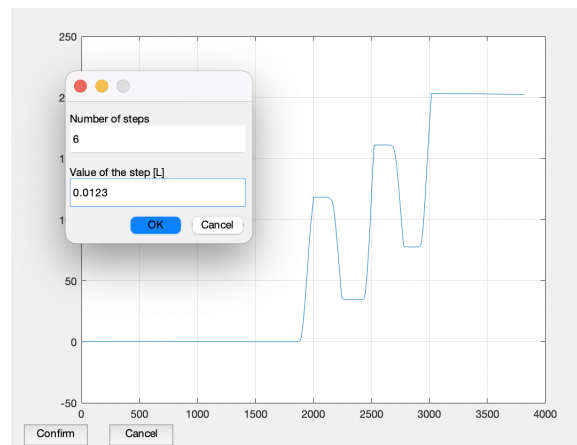

Figure 2.21: Plot of Integrated Flow with User-Provided Steps and Values.

integral of the signal, enabling the assessment of the cumulative volume over time. To facilitate this process, the user was prompted to input additional parameters, including the number of steps performed with the syringe and the corresponding volume used in liters (Figure 2.21). These steps were meticulously selected on the provided graph, ensuring the accuracy and reliability of the subsequent calculations.

Then the CalFlow function generated a supplementary image, presenting the flow values in L/s (Figure 2.22). With the confirmation of the converted flow values, the function proceeded to provide an illustrative graph, depicting the volume (as the integral of flow) in liters. Additionally, the function furnished the essential coefficients, denoted as m and q, enabling the subsequent conversion of pressure values expressed in digits into their corresponding flow values in L/s.
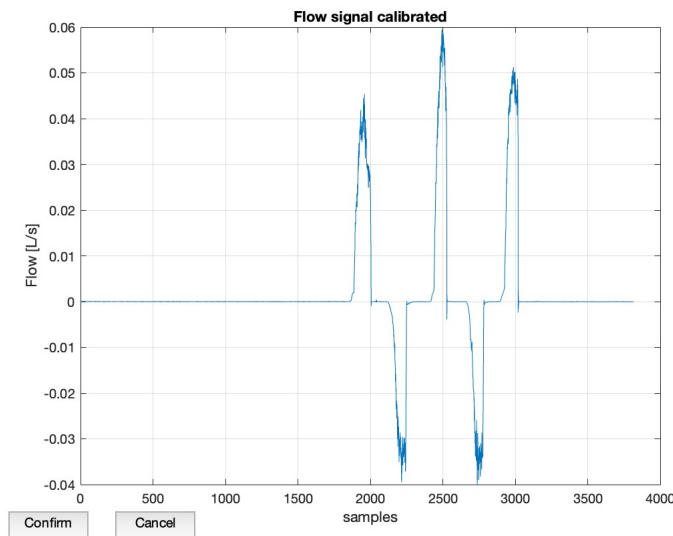
Figure 2.22: Plot of Calibrated Flow (L/s) vs. Samples.

In order to establish the quantitative relationship between the pressure in digit (x) and the corresponding flow (y), a linear equation of the form y = m*x + q was utilized. To mathematically validate this relationship, the values of m and q obtained from the calibration process were applied to calculate the flow values. Additionally, the "Cumtrap function" was employed to compute the integral of the flow, taking into account the period (representing the base of the trapezoid) and the flow values (representing the height). The resulting plot, showcasing the integral of the flow, exhibited remarkable similarity to the graph generated by the CalFlow function. This striking resemblance further confirmed the validity of the calibration procedure and the reliability of the derived linear equation.

2.5. Hardware

The hardware setup involves two distinct circuits connected by a long wire: one designed for the MRI room with non-ferromagnetic components, and the other located in the non-MR-compatible electronic module. The MRI-compatible circuit includes sensors and valves, while the electronic module circuit comprises Arduino, Raspberry Pi, a power supply, LEDs, switches, and a conditioning circuit for the differential pressure sensor. Arduino and Raspberry Pi are crucial in controlling and processing data, while the power supply ensures stable operation. LEDs provide visual feedback, and the conditioning circuit enhances the accuracy of pressure measurements.

In the context of the hardware setup, it is important to address the specific characteristics and requirements of the valves. These valves are equipped with two pins, each serving
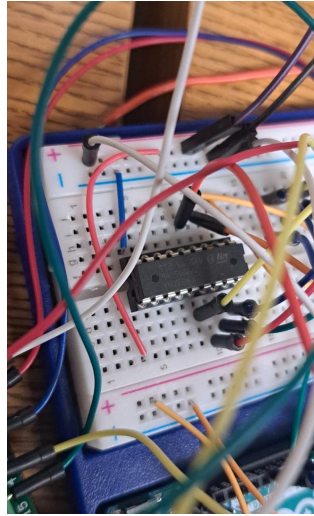
Figure 2.23: Darlington integrated circuit (IC), model is the ULN2804A by STMicroelectronics.

a distinct purpose in the overall functionality. One pin is designated for connection to the power supply, while the other is intended for integration with the Darlington transistor arrays. Furthermore, the valves necessitate a stable 12V power supply to operate efficiently. This implies that the power circuit must be designed to accommodate this voltage requirement, ensuring that both the 5V power supply for Raspberry Pi, Arduino, and various sensors, as well as the 12V supply for the valves, can be reliably provided. To safeguard the valves and the entire system from potential voltage surges, a protective measure in the form of a diode is incorporated into the valve circuit. This diode is strategically placed between the two Valves' PINs, effectively preventing excessive voltages that could potentially harm the valves.

Regarding the selection of the Darlington integrated circuit (IC), the chosen model is the ULN2804A by STMicroelectronics (Figure 2.23). This specific model offers a range of features and capabilities suitable for controlling high-current loads, such as relays, solenoids, and motors, through low-level control signals originating from a microcontroller or digital circuit. Furthermore, the ULN2804A incorporates built-in protection features, including diode clamps, which safeguard against voltage spikes and back electromotive force (EMF) generated by inductive loads. These protection mechanisms help to ensure the reliability and longevity of the circuit by preventing potential damage to both the IC and the connected high-current loads (Figure 2.24).

The ULN2804A consists of eight Darlington pairs, where each pair consists of a high-voltage, high-current Darlington transistor. These transistor pairs are capable of providing high current gain and can handle significant loads with minimal power dissipation. The
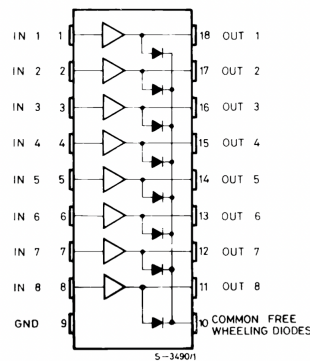
Figure 2.24: Darlington integrated circuit (IC), PIN connections.

IC is commonly used in various applications where multiple output channels are required, and it simplifies the interface between low-level control signals (such as those generated by microcontrollers) and high-power loads. Each Darlington pair in the ULN2804A can handle currents of up to 500mA and withstand voltages of up to 50V, providing the necessary amplification of current to meet the requirements of these loads.

To facilitate the power control functionality of the device, three switches have been incorporated. These switches serve distinct purposes, with one dedicated to managing the power supply, another responsible for activating the ventilator, and a third enabling the transition between the Normal mode and the HP (hyperpolarize) mode during the ventilation process. Furthermore, to provide visual feedback and status indication, two LEDs have been integrated into the system. A red LED signifies the Normal mode, while a yellow LED represents the HP mode.

In terms of the physical connections, the switches are connected from the firs terminal to the 5V power supply. From the other one, a 20K ohm resistor is introduced into the circuit before the connection is established with the input of the Arduino microcontroller. This setup ensures proper voltage regulation and signal conditioning for reliable operation. On the other hand, the LEDs are connected in series with a 200 ohm resistor. The anode of each LED is connected to the ground, while the cathode is connected to the resistor. This configuration allows for controlled current flow through the LEDs, preventing excessive current draw and ensuring their longevity. The resistor is then connected to a dedicated output pin of the microcontroller, enabling precise control of the LED illumination (Figure 2.25). The specific value of the resistor has been deliberately chosen after careful consideration and calculations to ensure optimal performance and adherence to the desired current levels. For further details and a visual representation of the circuit connections, please refer to the accompanying Figure 2.26.
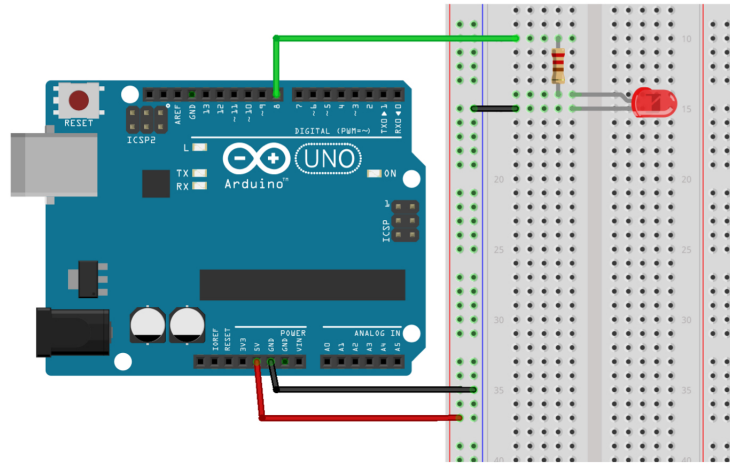
Figure 2.25: Circuit diagram illustrating the implementation of LEDs with appropriate current-limiting resistors.

Lastly, the final component incorporated in the electronic circuit, which cannot be located inside the MRI chamber, is the conditioning circuit for the differential pressure transducer, as discussed in the preceding chapter 2.4.1.

Regarding the MRI-compatible circuit, it comprises several essential components that are required to be located inside the MRI room. These components include the three pressure sensors, responsible for monitoring the pressure levels in each line, as well as the differential pressure transducer and the valves. The purpose of the breadboard in this setup primarily revolves around facilitating the interconnection of these sensors with the power supply and the second breadboard housing various conditioning circuits. Notably, the electronic components on this breadboard are limited to diodes. With respect to the differential pressure transducer, it is equipped with three pins, as depicted in the datasheet image provided in the appendix. The first pin is connected to a 5V power supply, the second pin is grounded, and the third pin is linked to the conditioning circuit. It is worth noting that all these MRI-compatible components are not directly linked to the electronic module. Instead, they are connected to this breadboard, and subsequently, a long 13-pin wire serves as a conduit for connecting them to the electronic module.

With regards to the individual pressure sensors by Fujikura Pressure Sensors, AG2 series, as indicated in their respective datasheets, they are equipped with three pins each (2.27). The first pin is connected to the ground, the second pin is designated as Vout (output voltage), and the third pin is connected to a 5V power supply. According to the specifications mentioned in the datasheet, it is recommended to connect a 0.1 microfarad capacitor

$$I_{LED} = 20 \ mA, V_{LED} = 1 \ V$$

$$V_{RES} = 5V \ - V_{LED} = 4 \ V$$

$$Res = \frac{V_{RES}}{I_{LED}} = \frac{4V}{20mA} = 200 \ \Omega$$

Figure 2.26: Determination of the resistor value for proper current flow in the LED circuit. Considering that the LED requires a current of 20mA and has a voltage drop of 1V, and taking into account the 5V power supply from Arduino, the remaining voltage across the resistor is 4V. To maintain a consistent current of 20mA, the appropriate resistor value is calculated based on Ohm's Law.
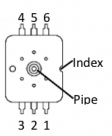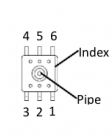
Pin Assignment		Pin No.	Pin Name	I/O	Type	Function
AP2	AG2					
		1	VSS	-	-	Common voltage connection
		2	VOUT	O	Analog	Analog output
		3	VDD	-	-	Power supply connection
		4	NC	-	-	-
		5	NC	-	-	-
		6	NC	-	-	-

Figure 2.27: PIN connection of the Fujikura Pressure Sensors, AG2 Series.

between the power supply and ground to stabilize the voltage. This capacitor has been duly incorporated into the breadboard of the electronic module, following the prescribed guidelines outlined in the datasheet. By implementing this capacitor, the voltage stability is enhanced, ensuring accurate and reliable measurements from the pressure sensors.

In terms of the power supply, an initial choice was made to utilize the laboratory's DC power supply (Figure 2.28), which was set to a voltage of 12V. The upper connections of the breadboard were carefully established with this power source to ensure a stable and reliable energy input. In addition, for the 5V power requirement, the power supply from Arduino itself was harnessed, providing a suitable voltage level for the various components and sensors integrated within the system.

To bolster the capacity of Arduino in handling the overall load, a 9V battery was incorporated. This additional power source played a pivotal role in ensuring adequate power
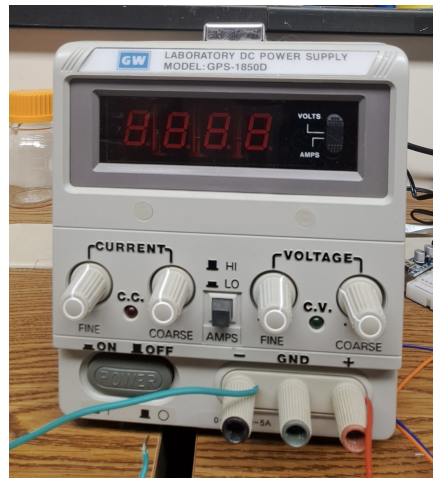
Figure 2.28: Laboratory's DC power supply to provide 12V.

distribution and management. Furthermore, Raspberry Pi, serving as an integral part of the system, received its power supply from a dedicated power adapter. This charger, directly connected to the mains power supply, delivered a consistent and reliable electrical current to sustain the operations of Raspberry Pi.

All the hardware used for the development of the ventilator is depicted in Figure 2.29. It is notable that the sensors are not directly connected to Arduino; instead, their pins are interconnected through the two breadboards using a long 13 pin wire.

2.5.1. PCB Development

In order to implement the hardware with a focus on ensuring ease of calibration a strategic decision was made to develop a dedicated Printed Circuit Board (PCB) for the pressure transducer's conditioning circuit. Developing a circuit on a Printed Circuit Board (PCB) offers several advantages over using a breadboard:

- Reliability and Durability: PCBs are designed for long-term use and are more durable than breadboards. Components are soldered onto the board, ensuring better contact and reduced risk of loose connections that can occur on a breadboard due to frequent handling.

- Compactness: PCBs allow for a much more compact and organized layout of components compared to breadboards, which can become messy and difficult to manage with complex circuits.

- Reduced Electromagnetic Interference (EMI): PCBs can be designed with specific ground planes and signal routing to minimize electromagnetic interference, making
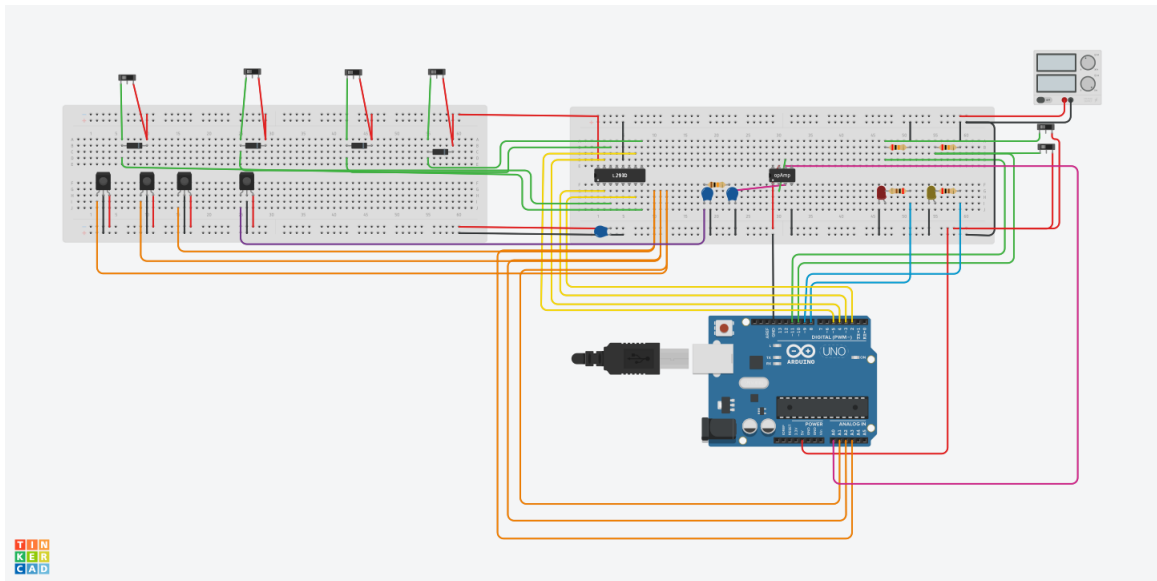
Figure 2.29: Ventilator hardware connections.

them suitable for applications where EMI is a concern. Breadboards, with their open and unshielded construction, are more susceptible to EMI.

- Customization: PCBs offer complete customization in terms of layout, size, and shape. This flexibility allows designers to create circuits tailored to specific project requirements, making them suitable for mass production.

- Higher Frequency Applications: PCBs are better suited for high-frequency applications due to their controlled impedance characteristics. Breadboards may introduce unwanted parasitic capacitance and inductance that can limit performance at high frequencies.

- Permanent Solution: PCBs are a permanent solution, whereas breadboards are typically used for prototyping and testing. Once a design is finalized, it can be easily replicated on PCBs for mass production.

- Environmental Considerations: Breadboards are often disposable and made from plastics, while PCBs can be more environmentally friendly if designed with recyclable materials and disposed of properly.

- Stability: Components on a PCB are less prone to movement or disconnection due to vibrations or mechanical stress, making them suitable for applications where stability is crucial.

For this purpose, we opted to utilize the PADS development environment, which offers two distinct environments: PADS Logic for the creation of the schematic and PADS

Layout for the assembly of components onto the board. The initial stages of this endeavor involved sourcing component footprints from online repositories and seamlessly importing them into the PADS Logic environment. Following this, the schematic was meticulously crafted, adhering closely to pre-established connections and guidelines derived from the initial breadboard configuration.

At the core of this hardware integration was the pressure transducer, a pivotal component in the overall system. It was skillfully integrated with the Arduino microcontroller through a specialized conditioning circuit. To achieve optimal electrical performance, the schematic design incorporated essential elements:

1. Power Supply Stabilization: To ensure a consistent and reliable voltage level, a 100nF capacitor was strategically placed between the ground and power lines. This stabilization was fundamental to reliable sensor operation.

2. Analog Output Optimization: A 10nF capacitor was thoughtfully integrated into the design, aligning with the precise specifications outlined in the sensor's datasheet. This capacitor played a critical role in fine-tuning the analog output.

3. Noise Attenuation: To further enhance signal quality and minimize interference from higher-frequency noise components, a 50 Hz low-pass filter was skillfully employed. This filter design was meticulously crafted, featuring the use of a 10Kohm resistor in conjunction with a 100nF capacitor to achieve the desired noise reduction.

In addition to these critical components, an operational amplifier (Opamp) was thoughtfully incorporated to ensure signal integrity and facilitate seamless interfacing with the Arduino's analog-to-digital converter (ADC). Specifically, the MCP6044-E/ST model from Microchip Technology was selected for its compatibility and performance characteristics. The Opamp was configured either as a Buffer or a Voltage Follower, optimizing the circuit for high input impedance and low output impedance. This configuration effectively allowed for the transmission of the sensor's signal to the ADC without introducing any compromise to the original signal integrity. It is possible to see the schematic in Figure 2.31.

With the hardware development phase successfully completed, the components were seamlessly exported to the PADS Layout environment to compose the final four-layer board. The trace layout and routing were meticulously developed, adhering rigorously to established PCB development principles. The end result of this process is visually evident in the provided Figure, reflecting the meticulous hardware integration efforts.
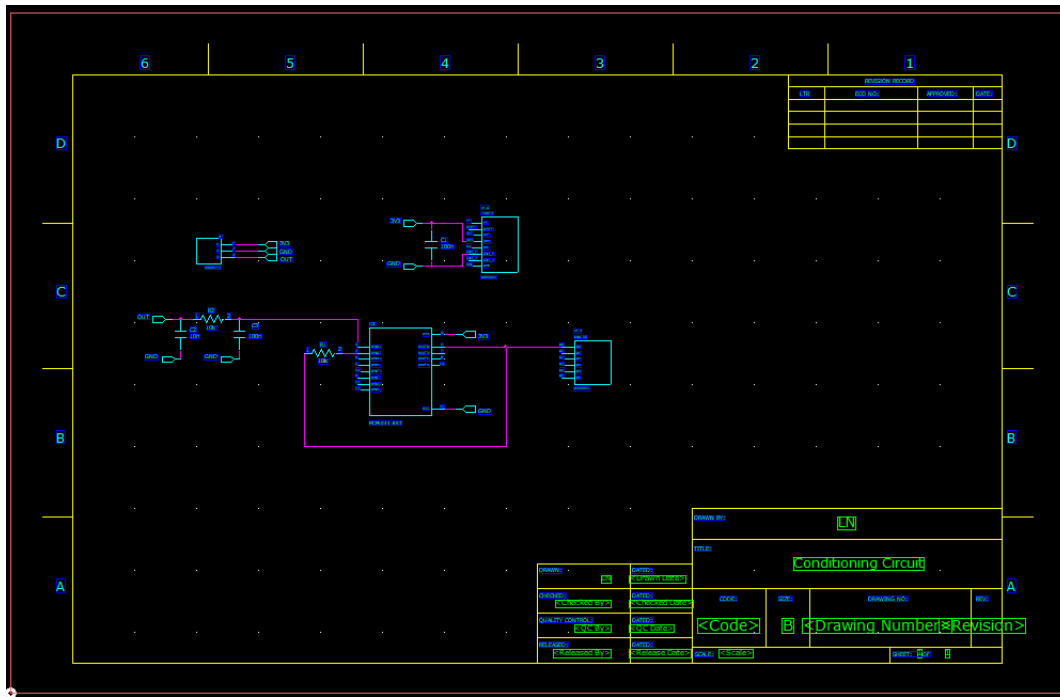
Figure 2.30: Conditioning Circuit Schematic made in PADS Logic.

2.6. Firmware

The Arduino Integrated Development Environment (IDE) was deliberately chosen as the programming platform for the development of the firmware responsible for controlling the ventilator. This decision was based on several factors, including the simplicity and versatility of the Arduino platform, as well as its compatibility with the specific requirements of the ventilator system. By leveraging the capabilities offered by Arduino, the firmware was designed and implemented to ensure precise control and seamless integration with the overall ventilator architecture.

The firmware code itself is structured into three distinct sections, each serving a specific purpose within the ventilator control process. It is worth noting that there exists an initialization phase wherein libraries are included, pin numbers are defined, and variables are initialized, there is an example in Figure 2.32.

The initial section, denoted as "void setup()," plays a critical role in the initialization phase. Within this section, all necessary configuration parameters are set, such as defining the input and output pins of the Arduino board and initializing the microcontroller's timer (Figure 2.33). These steps are crucial to ensure proper functioning and synchronization of the various components of the ventilator system. Moving on to the subsequent section, the "void loop()" function is intentionally left empty in order to adopt an interrupt-driven
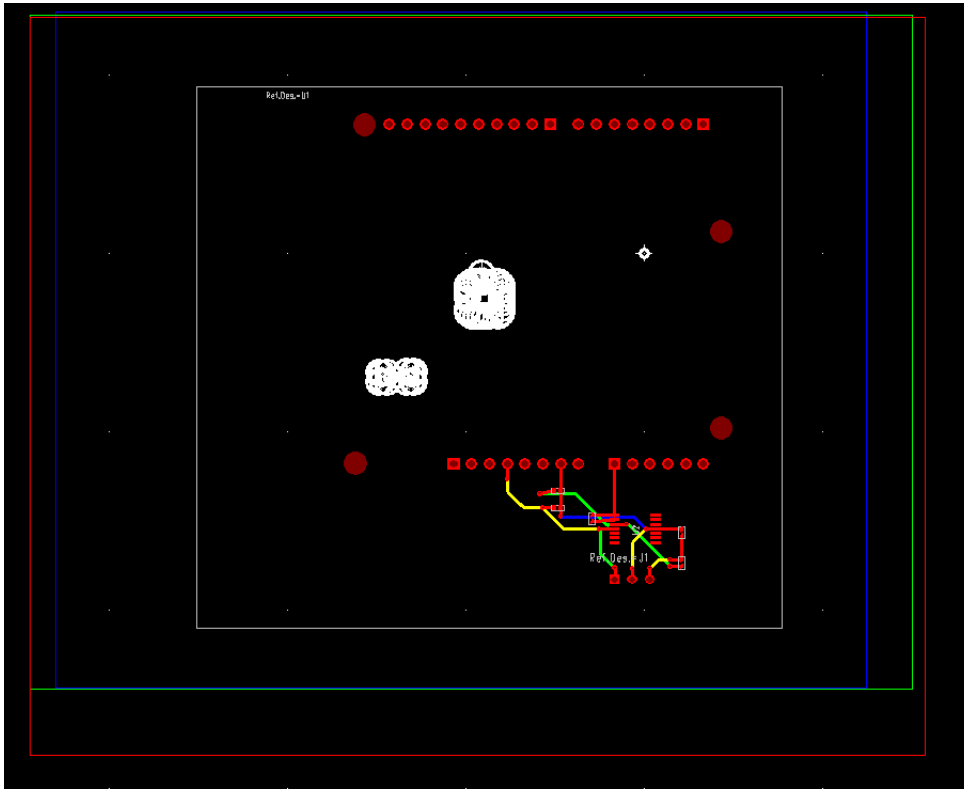
Figure 2.31: Four-Layer board made in PADS Layout.

approach, (Figure 2.34). This design choice allows for more precise control over timing and responsiveness within the firmware.

By utilizing the Interrupt Service Routine (ISR), the firmware can effectively handle time-sensitive operations, ensuring accurate and timely execution of the ventilator control logic. To facilitate effective management and operation of the ventilator, the firmware incorporates a state-based approach. This means that the firmware distinguishes between two primary states: the ventilator off state and the ventilator on state. In the ventilator off state, the firmware performs initial checks and measurements of critical parameters such as oxygen, nitrogen, and hyperpolarized gas pressure. These measurements serve as prerequisites for initiating the ventilator's activation process.

The measurements are being sampled based on the interrupt frequency of 250Hz, which has been previously defined. Upon entering this operational mode, the variable "count1sec" undergoes incremental changes, while these measurements are continuously acquired for a duration of one second. Once the value of "count" reaches 250, equivalent to the frequency of the Interrupt Service Routine (ISR), it signifies that a full second has transpired. At this juncture, the collected variables are averaged, and the resultant average values are forwarded to the Processing platform for visual representation on the monitor. Concur-

```
#include <avr/io.h>
#include <avr/interrupt.h>
#include "stdio.h"
#define analogPin A0 //pin number for differential pressure transducer
#define sensorO2 A3 //pin number for O2 pressure sensor
#define sensorN2 A1 //pin number for N2 pressure sensor
#define sensorHP A2 //pin number for HP pressure sensor
#define FREQISR 250 //sampling frequency
int O2pin =      5;       // the number of the Arduino I/O pin
int N2pin =      2;       // the number of the Arduino I/O pin
int HPpin =      3;       // the number of the Arduino I/O pin
int val=0; //variable that stores the diff pressure value
float O2=0; //variable that stores O2 pressure value
float HP=0; //variable that stores HP pressure value
float N2=0;//variable that stores N2 pressure value

float STARTBREATHHOLD = 0;
float STARTEXP = 0;
float ENDEXP = 0;
int count=0;
```

Figure 2.32: Initialization: libraries are included, pin names are defined, variables are initialized.

rently, the "count" variable is reset to zero, effectively initiating a fresh count for the ensuing second.

Upon meeting the specified requirements and validation criteria, the mechanical switch turn on the ventilator, thereby the firmware transits to the ventilator "ON State". Upon entering the "on" mode, the counter is incremented to manage the distinct phases of inspiration, breath hold, and expiration. Additionally, the differential pressure transducer is sampled, and its values are directly transmitted to the Processing platform, where the signal characterization takes place, Figure 2.36. This transmission part is well explained in Section 2.6.1.

Within the ventilator on state, the firmware further subdivides the operation into two distinct modes: the normal mode and the HP (hyperpolarized) mode. These modes are dynamically selected by another mechanical switch and are indicated by activating corresponding LED indicators, Figure 2.37. The firmware seamlessly manages the functionality and control aspects associated with each mode. In both the normal mode and the HP mode, the core functionalities and control procedures remain consistent. However, they diverge in terms of valve activation and pressure monitoring. In normal mode, the firmware closes the the HP valve and continuously monitors Nitrogen pressure instead of HP gas one, Figure 2.38.

On the other hand, in the HP mode, the firmware engages the solenoid valve, which subsequently triggers the Teflon valve, enabling the controlled release and monitoring of

```
void setup() {
  Serial.begin(115200);
  pinMode(O2pin, OUTPUT); //pin for O2 valve
  pinMode(N2pin, OUTPUT); //pin for N2 valve
  pinMode(HPpin, OUTPUT); //pin for the HP gas valve
  pinMode(ExhalePin, OUTPUT); //pin for the Exhale valve
  pinMode(sensorO2, INPUT); //pin for 02 pressure sensor
  pinMode(sensorN2, INPUT); //pin for N2 pressure sensor
  pinMode(sensorHP, INPUT); //pin for HP pressure sensor
  pinMode(analogPin, INPUT); //pin for differential pressure transducer
  pinMode(LEDN2, OUTPUT); //pin for normal mode led
  pinMode(LEDHP, OUTPUT); //pin for HP mode led
  pinMode(systemSwitch, INPUT); //pin for HP/normal mode switch
  pinMode(ONOFFSwitch, INPUT); //pin for ON/OFF switch
// initialize timer1
  noInterrupts();            // disable all interrupts
  TCCR1A = 0;
  TCCR1B = 0;

  TCNT1 = 65285;             // preload timer 65536-16MHz/256/250Hz
  TCCR1B |= (1 << CS12);     // 256 prescaler
  TIMSK1 |= (1 << TOIE1);    // enable timer overflow interrupt
  interrupts();
  }
```

Figure 2.33: Initial Section: 'void setup()' Configures Arduino's Pins and Timer.

```
void loop() {

}
```

Figure 2.34: Empty "void loop()" in order to use an interrupt-driven approach.

the hyperpolarized gas. These distinct operations in the two modes allow for adaptable and versatile ventilation strategies. The oxygen pressure, the oxygen valve, the exhale valve and the differential pressure transducer work in the same way in both modalities.

Regarding respiratory cycle management, the firmware incorporates a comprehensive approach to control the inhalation, breath hold, and exhalation phases. For instance, within the normal mode and considering that the ventilator is going to be tested on mice, during the 150ms inspiration phase, the firmware opens the oxygen and nitrogen valves while keeping the exhale valve closed, Figure 2.39. This facilitates the controlled intake of gases during the inhalation process.

Subsequently, in the 150ms breath-hold phase, all valves are closed, ensuring a temporary pause in the respiratory cycle, Figure 2.40. Finally, during the 300ms expiration phase, only the exhale valve is opened, allowing for the controlled release of gases from the system, Figure 2.41.

This well-defined and synchronized cycle, with a total duration of 600ms, enables the

```
if (digitalRead(ONOFFSwitch) == LOW){
  count1sec++;
  //THE THE VENTILATOR IS NOT WORKING
  //BUT WE WANT TO KNOW THE PRESSURE VALUE
    O2= analogRead(sensorO2); //reading the O2 sensor value
    Real_O2OFF = O2*0.00708884359726; //value given by calibration
    sumO2= sumO2 + Real_O2OFF; //all the values are summed

    N2= analogRead(sensorN2);
    Real_N2OFF = N2*0.0140540406977;
     sumN2= sumN2 + Real_N2OFF;

    HP= analogRead(sensorHP);
    Real_HPOFF = HP*0.0140540406977;
    sumHP= sumHP + Real_HPOFF;

    if (count1sec==FREQISR) {//1 second reached
     avgO2=sumO2/FREQISR; //average of O2
     avgN2=sumN2/FREQISR;
     avgHP=sumHP/FREQISR;
     sumO2=0;
     sumN2=0;
     sumHP=0;
     count1sec=0;
```

Figure 2.35: Ventilator OFF State: pressure in each line is acquired.

```
else {
//VENTILATOR ON
 count++;
  val=analogRead(analogPin); //reading the analog value
  Serial.print("Analog reading:"); //sending to processing
  Serial.print(",");
  Serial.print(val);
  Serial.print("\n");
```

Figure 2.36: Ventilator ON State: differential pressure is sampled and sent to Processing.

achievement of a desired breathing frequency, typically set to 100 breaths per minute. At this stage, as we reach the end of each cycle, several steps are carried out to ensure the smooth progression of the system. Firstly, the average pressure values obtained during the cycle are sent to the Processing platform. This transmission serves as a critical indicator, alerting Processing that the current cycle has concluded, thereby providing Processing with the necessary information for future command execution and subsequent operations. Moreover, this stage signifies a pivotal moment as the "count" variable is reset to zero, effectively preparing it for the commencement of a fresh counting cycle.

Therefore, this synchronization of data transmission, accompanied by the reset of the count, establishes a seamless workflow, enabling the system to operate reliably and consistently for the initiation of a new cycle.

```
//VENT ON
  if (digitalRead(systemSwitch) == LOW){
  ventMode = 0; //normalmode
  }
  else
  ventMode=1; //HP mode
```

Figure 2.37: Ventilator Modes selected by the switch.

```
if (ventMode == 0){ //Normal Mode
  digitalWrite(LEDN2, HIGH); //LED N2 ON
  digitalWrite(LEDHP, LOW);  //LED HP OFF
  digitalWrite(HPpin, LOW); //HP VALVE CLOSE

  O2= analogRead(sensorO2); //reading the O2 sensor value
  Real_O2OFF = O2*0.00708884359726; //value given by calibration
  sumO2= sumO2 + Real_O2OFF; //all the values are summed

  N2= analogRead(sensorN2);
  Real_N2OFF = N2*0.0140540406977;
  sumN2= sumN2 + Real_N2OFF;
```

Figure 2.38: Normal Node.

2.6.1. Communication between Arduino IDE and Processing

In this section, the communication protocol between Arduino and Processing, known as serial communication, will be explained. This communication protocol enables the exchange of information, allowing Arduino to transmit data to Processing and create the user interface. By leveraging serial communication, the collected data can be effectively displayed through graphical representations on a monitor.

To provide a comprehensive overview, let's delve deeper into the details. The data transmitted to Processing encompasses a range of measurements crucial for analysis and visualization. These measurements include the bit value of the differential pressure transducer, as well as pressure values of nitrogen, oxygen, and high-pressure (HP) gases, both during the ventilator's inactive and active states. In total, this entails a collection of seven distinct measurements. When transmitting multiple measurements, it becomes imperative for Processing to accurately comprehend the nature of the data being relayed and its corresponding value. To ensure seamless communication and facilitate proper data interpretation, a well-defined and structured setup has been established.

This setup involves a stringent protocol for transmitting the data in a systematic manner. It adheres to a predefined sequence depicted in the accompanying Figure 2.42. The transmission sequence entails several crucial steps: first, the name of the variable associated

```
if (count<STARTBREATHHOLD*FREQISR) { //inspiration
  digitalWrite(O2pin, HIGH); //O2 valve is open
  digitalWrite(N2pin, HIGH); //N2 valve is open
  digitalWrite(ExhalePin, LOW); //Exhale valve is closed
 }
```

Figure 2.39: Inspiration Set Up.

```
if (count>STARTBREATHHOLD*FREQISR && count<STARTEXP*FREQISR) { //breathold
  digitalWrite(O2pin, LOW);
  digitalWrite(N2pin, LOW);
  digitalWrite(ExhalePin, LOW);
}
```

Figure 2.40: Breath Hold Valves Set Up.

with the measurement is transmitted. This is followed by a comma, which serves as a designated separator character, clearly demarcating the variable name and its subsequent value. Subsequently, the actual value of the variable is transmitted. Finally, an "enter" or "carriage return" signal is sent to indicate the completion of the current variable's transmission and to signify the transition to the next variable.

This meticulous approach guarantees that Processing receives the data in a structured and organized format. By adhering to this protocol, the transmission process ensures that each variable's name and value are properly associated, allowing for accurate data processing and meaningful analysis in the subsequent stages. At this point, it is essential to analyze how Processing receives and interprets the transmitted data. Within the Processing environment, a function called "serialEvent" has been implemented, which takes the communication port connected to Arduino as its input parameter. This function plays a pivotal role in handling the incoming data.

Once the user initiates the data transmission by pressing the start button on the user interface (see 2.7), the serialEvent function starts reading the data string until it encounters the new line character. If the string is not empty, further processing is performed. At this stage, the string is split into two parts using a designated separator character, which in this case is a comma. The first part of the string is then matched against predefined variable identifiers sent by Arduino, as illustrated in the accompanying image 2.43 For instance, if the first part of the string matches "O2 pressure," the second part of the string, representing the corresponding value, is converted from a string to a float data type. This converted value is then stored in a user-defined variable for subsequent usage and analysis.

```
if (count>FREQISR*STARTEXP && count<FREQISR*ENDEXP) { //expiration
  digitalWrite(O2pin, LOW);
  digitalWrite(N2pin, LOW);
  digitalWrite(ExhalePin, HIGH);

}
```

Figure 2.41: Expiration Valves Set Up.

```
Serial.print("O2 pressure:");
Serial.print(",");
Serial.print(Real_O2);
Serial.print("\n");

Serial.print("N2 pressure:");
Serial.print(",");
Serial.print(Real_N2);
Serial.print("\n");
```

Figure 2.42: Serial Communication Protocol.

By implementing this logic within the serialEvent function, Processing effectively receives and interprets the transmitted data from Arduino. This process allows for the identification and extraction of specific measurements based on predefined variables, enabling further manipulation, visualization, and analysis within the Processing environment.

In order to enhance the flexibility and adaptability of the ventilator system, particularly to cater to various types of animals, a two-way communication channel has been established between Processing and Arduino. The user interface serves as the primary platform for configuring the ventilator settings. On the initial screen of the interface, the user is presented with several input fields, including the duration of inspiration, expiration, and breath-hold phases. These parameters play a crucial role in determining the timing and characteristics of the ventilation process. By providing these input fields, the interface empowers the user to customize the ventilator's operation to suit the specific needs of different animals or respiratory conditions.

Upon entering the desired parameter values into the text input fields, the values are captured and converted into integer format. This ensures compatibility with the communication protocol between Processing and Arduino. Subsequently, the interface initiates the transmission of these parameter values to Arduino.

To facilitate the communication process, a specific format is employed. The parameter values are sent to Arduino as a single value, separated by a comma as it is possible to see in Figure 2.44. This format enables Arduino to accurately extract and interpret each

```
if(a[0].equals("O2 pressure:")){
   inString = trim(a[1]);
   inByte1 = float(inString);
```

Figure 2.43: Processing Code snippet showcasing string recognition and conversion to float data type for further processing.

```
String insp_str= insp_field.getText();
String exp_str= exp_field.getText();
String breathhold_str= breath_hold_field.getText();

int saved_insp = Integer.parseInt(insp_str);
int saved_exp = Integer.parseInt(exp_str);
int saved_breathhold = Integer.parseInt(breathhold_str);

myPort.write(saved_insp + "," + saved_breathhold + "," + saved_exp);
```

Figure 2.44: Processing Code to send data to Arduino.

parameter value during the data reception process. The comma serves as a delimiter, marking the boundaries between individual values within the transmitted string. Arduino, upon receiving the parameter values, processes and incorporates them into the ventilator's control algorithm. The updated parameters govern the timing and duration of the various respiratory phases, dynamically adapting the ventilation process to match the user-defined specifications. This ensures that the ventilator operates in accordance with the desired settings and accommodates changes or adjustments made by the user during the respiratory cycle.

Within the code, we can observe that these user-defined variables are received as soon as the interrupt service routine (ISR) begins execution. Upon reception, these variables undergo a conversion process to ensure their consistency and usability throughout the ventilator system. The user interface prompts the user to input the parameter values in milliseconds, reflecting the desired durations for various phases of the respiratory cycle. These values are then divided by 1000 to convert them from milliseconds to seconds, as the ventilator system operates based on second-based timing.

It is important to note that the code utilizes cumulative timing, rather than absolute time values. For instance, in it is not used the duration of inspiration such as 150 milliseconds. Instead, the timing of each phase is calculated cumulatively based on the preceding phases. This approach ensures that each phase of the respiratory cycle starts and ends at specific moments, rather than focusing solely on its duration. For example, the timing for the start of expiration is determined by summing the duration of inspiration and the breath-hold period, while the timing for the end of the expiration is the sum of all the values

```
String insp_str= insp_field.getText();
String exp_str= exp_field.getText();
String breathhold_str= breath_hold_field.getText();

int saved_insp = Integer.parseInt(insp_str);
int saved_exp = Integer.parseInt(exp_str);
int saved_breathhold = Integer.parseInt(breathhold_str);

myPort.write(saved_insp + "," + saved_breathhold + "," + saved_exp);
```

Figure 2.45: Arduno code to manage data received by Processing.
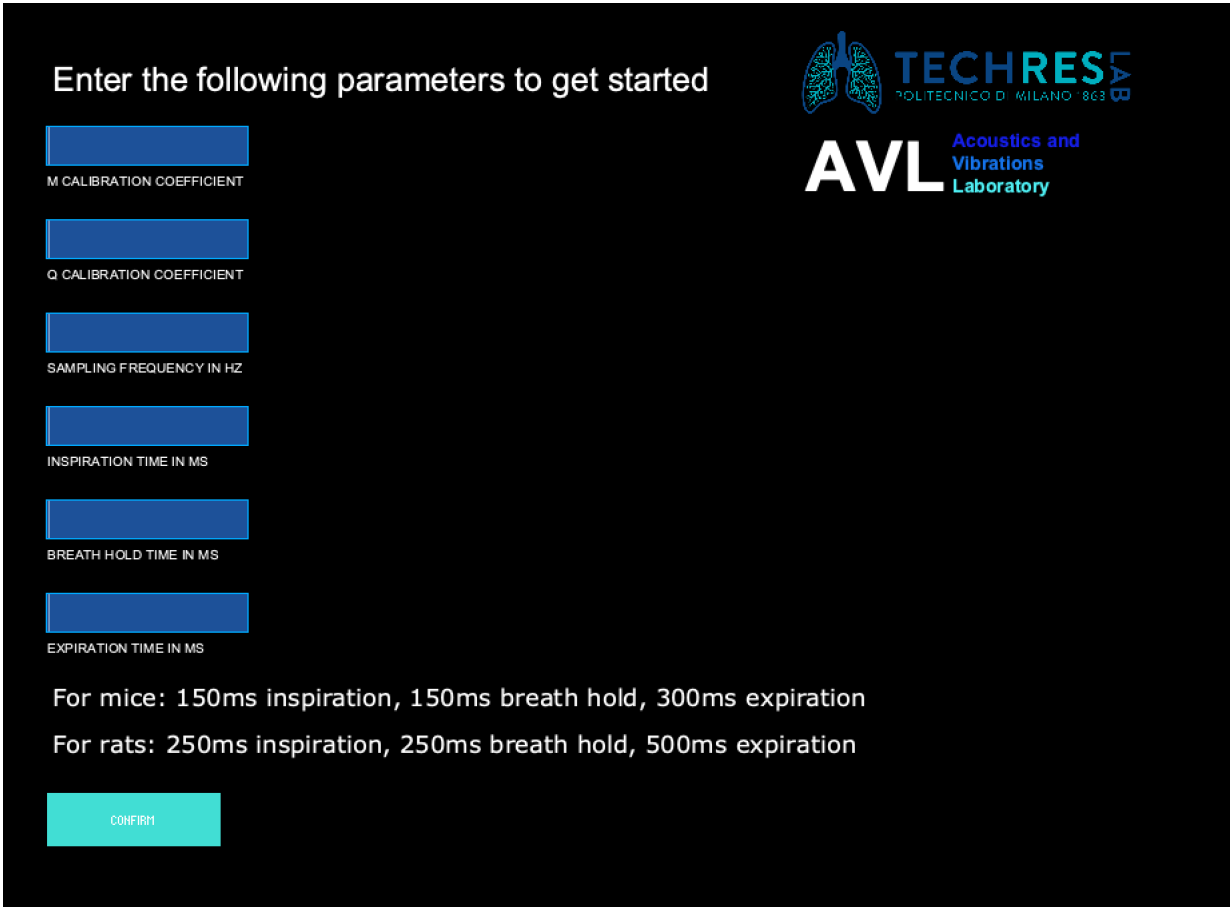
(inspiration, breath-hold, and expiration duration), Figure 2.45.

2.7.   User Interface

The user interface for the ventilator system was implemented using the Java programming language through the Processing framework. Processing, known for its versatility in creating interactive visual applications, provided a robust foundation for developing a graphical user interface (GUI) with enhanced functionality. Before delving into the explanation of the user interface, it is important to clarify that the data displayed in the user interface was primarily for visualization purposes and not indicative of the actual volumes and pressures administered to laboratory mice. The focus was on showcasing the functionality of the interface rather than providing accurate measurements. This transparency ensures that users understand the purpose of the interface and can appropriately set parameters for their experiments.

As it is possible to see from the Figure 2.46, the initial screen of the interface presents users with a comprehensive set of parameters to configure. These parameters encompass crucial aspects such as the calibration coefficients, denoted as 'm' and 'q', which play a pivotal role in deriving accurate flow measurements from the differential pressure transducer readings (see Section 2.4.1). Additionally, users are prompted to specify the desired sampling frequency, a crucial factor for accurately calculating the tidal volume based on the measured flow data.

To ensure flexibility and adaptability, as already said in the previous section, the user interface also offers the ability to set inspiration, breath-hold, and expiration times, allowing customization of the respiratory cycle according to specific requirements. Notably, the interface incorporates a helpful reminder section at the bottom, displaying established timing values utilized in the relevant scientific literature for mice and rats, serving as a valuable reference for users. Beyond its functional components, the interface showcases

Figure 2.46: User Interface first page: the user is asked to insert different parameters.

the collaboration between two reputable laboratories involved in the development process. The TechRes Lab at Politecnico di Milano and the Acoustic and Vibration Laboratory at UIC are acknowledged through the inclusion of their respective logos.

Upon inputting the necessary parameters and confirming the settings, a seamless transition occurs, leading to the appearance of a new screen. This screen encompasses additional functionality by including two prominently displayed buttons: Start and Stop. Once the Start button is pressed, data transmission begins from Arduino to Processing, triggering the display of the third page in the user interface.

It is important to note that, as mentioned in the hardware section 2.5, the ventilator is equipped with mechanical switches and its power on/off operation is controlled by them. Thus, in the firmware Arduino, based on the signals received from the switches, determines the current state of the ventilator. As discussed in the hardware section, at the initial stage of operation, all valves within the ventilator system are intentionally kept deactivated, resulting in the absence of any airflow. This deliberate configuration allows

Table 1   Size of Restrictors, Supply Pressure, and Ventilation Parameters for Mice and Rats

	Mouse						
	Orifice Diameter (mm)	Supply Pressure (psig)	Breathing Rate (min^{-1})	Inhalation Duration (ms)	Breath Hold Duration (ms)	Expiration Duration (ms)	Tidal Volume (ml)
O_2	0.02	2.0	100	150	150	300	0.05
N_2	0.04	3.0					0.20
^{3}He	0.04	3.5					0.20
^{129}Xe	0.07	4.5					0.20

	Rat						
	Orifice Diameter (mm)	Supply Pressure (psig)	Breathing Rate (min^{-1})	Inhalation Duration (ms)	Breath Hold Duration (ms)	Expiration Duration (ms)	Tidal Volume (ml)
O_2	0.13	6.0	60	250	250	500	1.0
N_2	0.24	5.0					3.0
^{3}He	0.22	4.0					3.0
^{129}Xe	0.26	3.5					3.0

Figure 2.47: Pressure requirements to achieve the specific Tidal Volume for mice and rats.

for thoroughly verifying and validating the pressure readings throughout the system. Monitoring and controlling the pressures are of utmost importance, as they serve as the primary determinant for achieving the desired volume delivery.

In the case of the Noulset-All ventilator [16], specific pressure thresholds have been established to ensure precise volume control, tailored to meet the respiratory requirements of small animals. For instance, as it is possible to see in this image 2.47, in order to achieve an Oxygen tidal volume of 0.05 ml for a mouse, it has been determined that a consistent pressure level of 2 pounds per square inch (psi) is necessary within the oxygen line. By maintaining this pressure, the ventilator can reliably deliver the desired volume, enabling efficient and accurate respiratory support.

In the displayed screenshot 2.48, the user interface shows the ventilator in the off state, indicating zero airflow, while various pressures are being monitored. In this case, only the nitrogen line was connected to the laboratory air, while the other lines were not supplied with air. As a result, the nitrogen pressure is registered at 4 psi, while the other lines indicate a pressure of approximately 0 psi.

Once the pressures were verified to align with the expected tidal volumes, the ventilator could be activated using the manual switch. As mentioned earlier, the type of gas delivered to the mouse, whether N2 or Xenon, depended on another switch. Consequently, depending on this setting, two different screens would appear in the interface: HP mode OFF, Figure 2.49, or HP Mode ON, Figure 2.50.

In the HP mode OFF that represents the Normal Mode ventilation, since we had activated
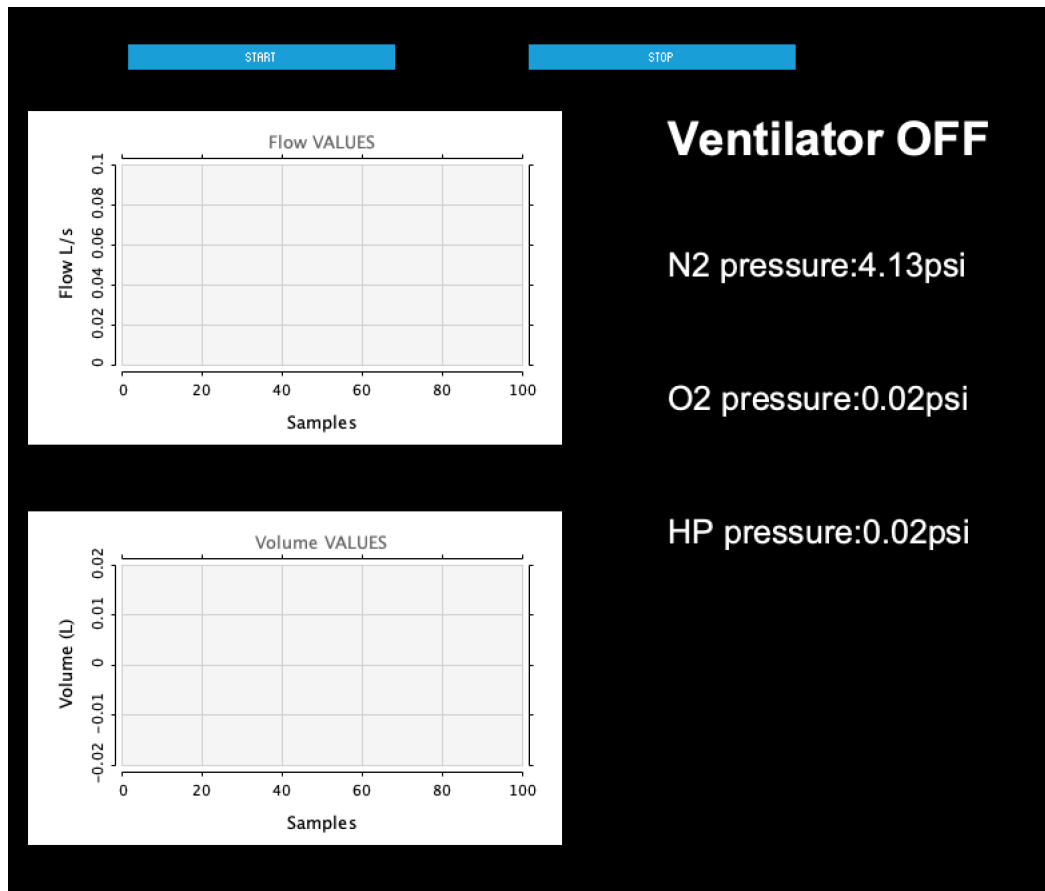
Figure 2.48: Ventilator in Off State: Monitoring Various Pressures with No Airflow.

the airflow in the nitrogen line previously, we can observe graphs displaying the flow and volume, along with the nitrogen and oxygen pressures. Conversely, in the HP Mode, the flow value would be zero as the nitrogen valve would be closed. Furthermore, since we did not activate any other lines, all the pressure values for oxygen and Xenon would be zero, indicating no airflow in these lines.

During the data visualization process, it is crucial to consider the timing at which the various data points are presented. Specifically, the flow and volume graphs are updated in real-time, ensuring a dynamic representation of the changing values. This real-time update is achieved by sending the differential pressure readings within the interrupt, which occurs at a rate of 250 times per second.

On the other hand, when it comes to displaying the pressure values for flow and volume, a different approach is taken. These values are shown specifically at the end of expiration, providing a comprehensive view of the respiratory cycle. The coordination between Arduino and Processing plays a crucial role in this process.
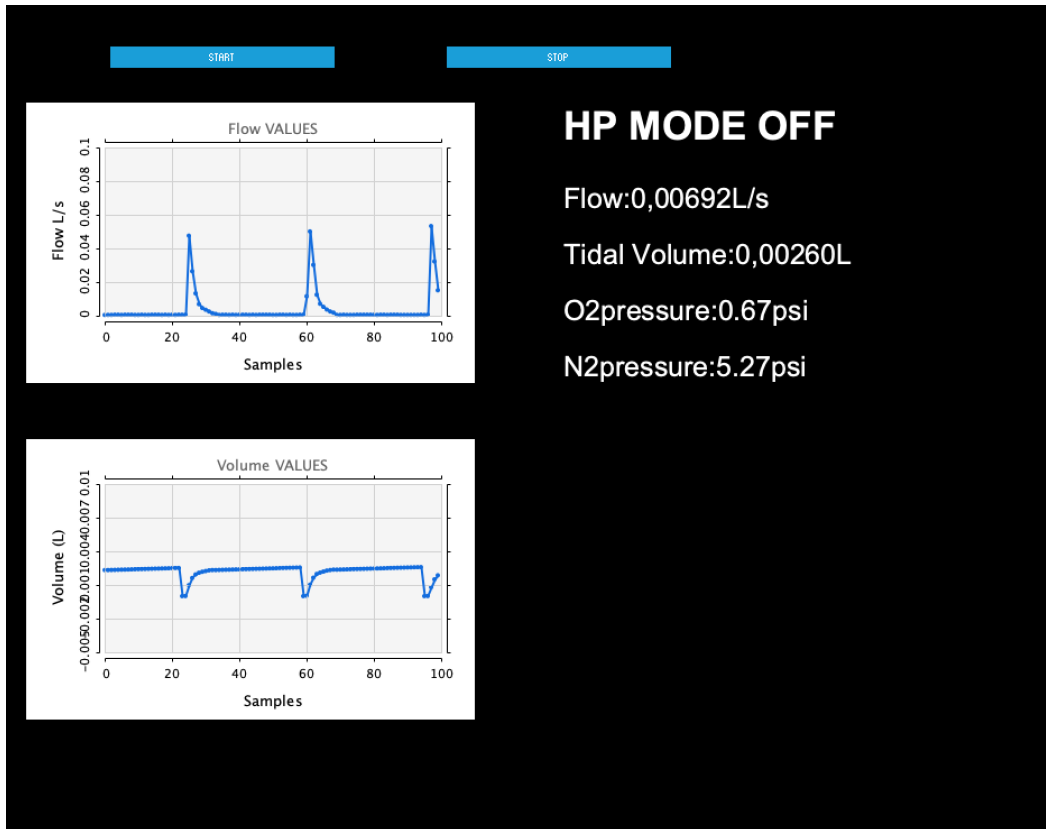
Figure 2.49: The interface displays the Ventilation during normal ventilation, with flow and volume graphs and nitrogen pressure.

Arduino, being responsible for capturing the relevant data, calculates and sends the average pressure value at the end of each breathing cycle. This average value serves as a clear indicator that expiration has ended. Upon receiving this information, Processing raises a flag to signify the end of expiration and subsequently triggers the display of the corresponding pressure, flow, and Volume values. Once the values are displayed, the flag is reset to zero, preparing the system for the next cycle of data acquisition and visualization.

As previously discussed, ensuring accurate pressure values is crucial to the achievement of the desired tidal Volume. However, an equally critical aspect that demands meticulous attention is the management of airflow and the subsequent determination of volume. Achieving optimal ventilation requires a comprehensive comprehension of the complex relationship between airflow rates, pressure differentials, and volume delivery. This topic will be extensively explored in the next chapter, given its fundamental role in the development of mechanical ventilators.
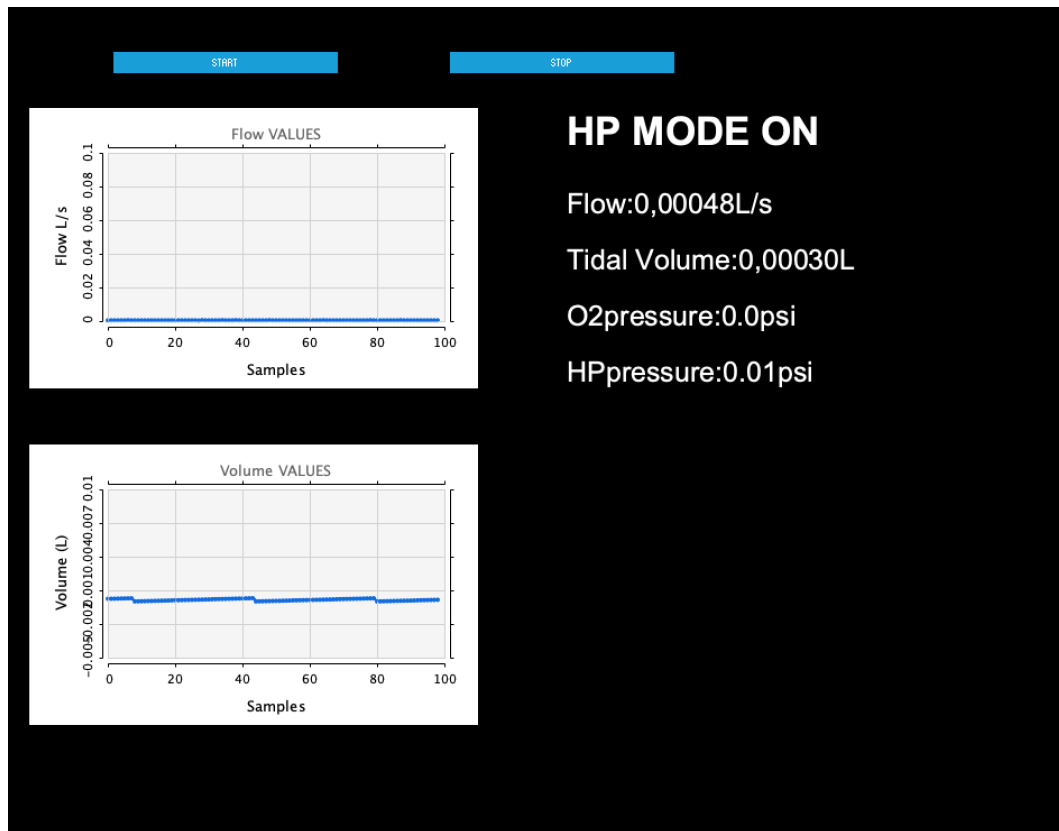
Figure 2.50: The interface displaying the Ventilation during HP mode, with zero flow and zero pressure values for Xenon and oxygen lines.

2.8.   Airflow and Volume Management

Before delving into the process of validation, it is crucial to thoroughly comprehend the relationship between airflow and volume and emphasize the methodology employed to calculate these parameters accurately. As previously highlighted (see 2.4), the determination of airflow relies on the utilization of a Pneumotachometer (PNT), and the interplay between airflow, resistance, and pressure can be analogized to the correlation between current, resistance, and voltage drop in the realm of electrical engineering. Notably, when an electric current traverses a resistor, it induces a voltage drop across the resistor. Similarly, in the context of airflow, the passage of air through a resistance generates a discernible pressure differential across the resistance.

Consequently, the pneumotachometer leverages this approximated linear relationship between airflow and pressure, enabling the derivation of coefficients, denoted as m and q, through a linear regression model of the form y = mx + q. The explanation of how these coefficients were obtained has already been addressed in the calibration section (2.4.1).

```
if(a[0].equals("Analog reading:")){
    inString = trim(a[1]);
    inByte= float(inString); //trasform pressure in int
    prev_flow=flow;//save flow in pre flow
    flow = saved_m * inByte + saved_q; //compute the new flow
    String shortflow = nf(flow, 0, 5); //make it with 5 decimals
    flowtext.setText("Flow:" +shortflow +"L/s"); //print it
```

Figure 2.51: Implementation of code for computing airflow based on the bit value from the differential pressure transducer. The calculated airflow is then displayed on the user interface screen.

Within the context of this section, our focus shifts towards elucidating how these derived coefficients are effectively employed to ascertain airflow. Beginning with the firmware's initial screen, the user is prompted to input the obtained coefficients, namely m = 0.000117 and q = 0.052207. These user-defined values are then diligently saved and effectively combined within the firmware's computational framework to yield the precise airflow measurement in units of liters per second (L/s), Figure 2.51.

At this stage, once the flow has been calculated, it is important to understand the relationship between flow and volume. In many cases, the flow is measured and needs to be integrated over time to obtain the volume. Numerical integration methods come into play, wherein adjacent data points are connected by a curve, and the areas under each curve segment are calculated and summed. Various numerical integration methods are available, with differing levels of sophistication. More advanced algorithms offer more accurate interpolations between data points but often involve increased complexity.

One of the simplest numerical integration methods is the trapezoidal rule, which approximates the area under the curve by dividing it into trapezoids. This method involves calculating the sum of the areas of these trapezoids, yielding an estimation of the integrated value. In the specific case of airflow and volume measurement, the trapezoidal rule is applied to integrate the measured flow over time. As depicted in the Figure 2.52, The flow signal (V') is integrated by joining its data points using straight lines and calculating the area under each line segment. By dividing the acquisition time into segments between measurements, this value corresponds to the height of our trapezoid. As for the bases of the trapezoid, the first base is determined by the flow value at the time "i", while the second base is determined by the flow value at the subsequent time. The gray area represents the incremental volume between two consecutive measurements, therefore, the cumulative volume can be computed by summing these segment areas.

$$V = V_0 + \sum_{i=1}^{n} \Delta V_i$$

$$\Delta V_i = \Delta t \, (V'_i + V'_{i-1})/2$$
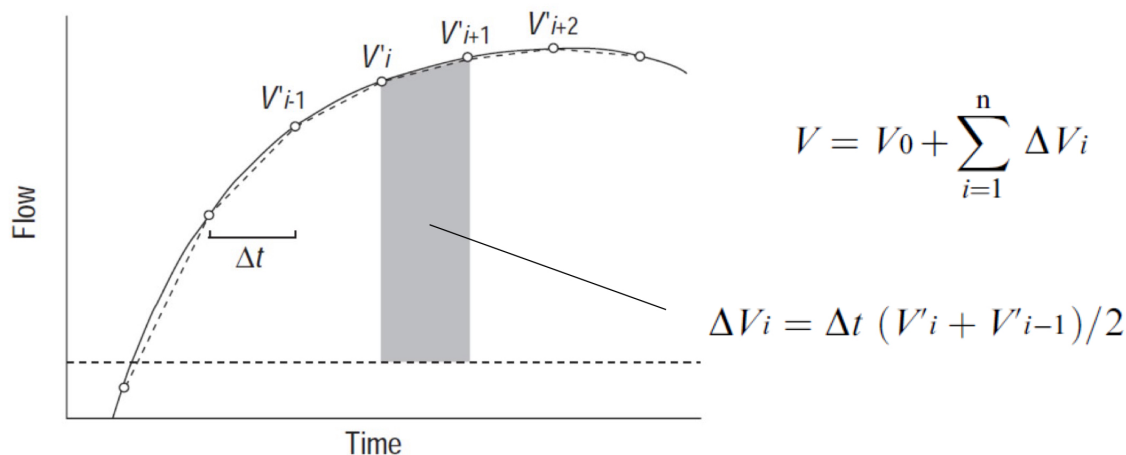
Figure 2.52: Illustration of the Trapezoidal Rule.

In the code implementation, the trapezoidal rule is incorporated as follows: firstly, the previous flow value is stored, serving as the first base of the trapezoid. Then, the new flow value is calculated, determining the second base. Regarding the time interval, the user is prompted to input the sampling frequency. The interval between two consecutive measurements is then computed as the reciprocal of the sampling frequency, representing the time span for each segment and the trapezoid height. With these values in place, the trapezoidal rule formula is applied, taking into account the division by two to calculate the incremental volume for each segment. The cumulative volume is obtained by summing up all these incremental areas, yielding the total volume, Figure 2.53.

2.9.   End-Expiratory Pressure Management

To establish a favorable positive end-expiratory pressure at the oral cavity of the subject, diverse strategies have been explored. This constitutes a pivotal component within the mechanical ventilation apparatus, ensuring that lung pressure remains above ambient levels subsequent to exhalation. This action serves to elevate the functional residual capacity (FRC), thereby augmenting the available surface area for efficient gas exchange. Additionally, it proactively safeguards the lung from ventilation-induced lung injury (VILI) by circumventing the cyclic opening and closure of unstable pulmonary units[23].

The expiratory branch is subjected to this pressure through a variety of approaches. The same processes controlling the complete respiratory circuit directly achieve this goal in the case of pressure-controlled ventilators. As an alternative, a widely used solution is using a voice coil motor to control a disc valve. This valve, which controls outward airflow and

```
if(a[0].equals("Analog reading:")){
    inString = trim(a[1]);
    inByte= float(inString); //trasform pressure in int
    prev_flow=flow;//save flow in pre flow
    flow = saved_m * inByte + saved_q; //compute the new flow
    String shortflow = nf(flow, 0, 5); //make it with 5 decimals
    flowtext.setText("Flow:" +shortflow +"L/s"); //print it
    area_flow= deltatime * (flow+prev_flow) / 2.0; //Applying the trapezoidal rule
    Volume= Volume+area_flow; //summing small Volumes
    area_flow=0; //reset this at zero after the sum

    if(flag_endexp) {
      String shortVolume = nf(Volume, 0, 5); //make it short
      Volumetext.setText("Tidal Volume:" +shortVolume +"L"); //print the volume
      Volume=0;
      flag_endexp=false;
    }
}
```

Figure 2.53: Code for computing volume from flow measurements using the trapezoidal rule.

is located along the expiratory branch, requires perfect disc movement synchronization with the flow pattern in order to maintain consistent end-expiratory pressure.

When dealing with the respiratory rates required by small animals, where up to 300 respiratory cycles per minute are often seen, this task becomes much more difficult.

The Bubble-Continuous Positive Airway Pressure method is a straightforward yet effective technique that offers a safe and practical way to provide continuous positive airway pressure (CPAP). Hydrostatic pressure is applied to the complete respiratory circuit by submerging the expiratory end limb and channeling it via an underwater seal.

$$P = \rho g h$$

ρ stands for liquid density, g for gravity's acceleration, and h for the liquid column's height above the inspiration limb end. A minimal pressure differential arises at the animal's airway opening as the equilibrium is approached between the pressure within the water column and the pressure within the expiratory limb. The quantity of water submerged at the distal end of the limb, typically ranging from 3 to 10 cmH2O, can be easily adjusted to regulate the applied pressure[23].

The exhaled air, as it passes through the system, is released in the form of bubbles, thus preventing the occurrence of airway obstruction due to excessive pressure.

Given its mechanical nature, this method operates independently of any synchronization with the subject's breathing pattern and generates a pressure that exhibits only slight variability, primarily influenced by a single factor.

3 | Validation

This chapter aims to provide a comprehensive overview of the validation process for the ventilator system, aiming to ensure its functionality and reliability. The validation procedure encompasses various aspects, beginning with the setup phase, and implementing newly developed codes that enhance its performance and accuracy. Moving forward, the focus shifts toward the validation of crucial components and parameters. Firstly, the validation of the pressure transducer takes place, followed by the validation of the Pneumotachometer (PNT) then the validation process extends to assessing the timing and efficiency of the valve opening mechanism.

It is important to acknowledge that during the validation process, the unavailability of flow restrictors posed certain limitations. As a result, a comprehensive validation of the entire ventilator system could not be conducted at that time. However, significant efforts were made to validate and assess the individual components and subsystems of the ventilator, providing valuable insights into their performance and contributing to the overall understanding of the system's behavior. In the subsequent discussion section, a more detailed analysis and reflection on the limitations and implications of the partial validation process will be presented. This comprehensive examination will shed light on the significance of future investigations and improvements, highlighting the need for further validation procedures and the potential impact on the overall performance and functionality of the ventilator system.

3.1. Validation Set Up

Regarding the utilized setup, the hardware connections remained consistent with those described in the hardware section. However, concerning the tube connections, the laboratory faucet was connected to a tube, which was then connected to the regulator attached to the N2 valve. Between the regulator and the valve, the pressure transducer was placed in series with a commercial digital pressure transducer, in order to see if this sensor was displaying the right pressure. At the outlet of the N2 valve, the pneumotachometer (PNT) was attached, and the tube from the PNT terminated in an aquarium with an inverted

Figure 3.1: The cylinder visually represents the measured air volume from the PNT.

graduated cylinder filled with water. The concept behind this setup was for the PNT to register the same volume of air that was being depleted in the cylinder, Fig. 3.1.

This experiment was conducted with various pressures ranging from 5 psi to 1 psi, with an interval of 0.5 psi. For each pressure, three sets of 10 respiratory cycles were performed. At the conclusion of these 10 cycles, the volume variation in the water cylinder was recorded and compared with the reading from the PNT. Therefore, this process was repeated three times, and the average of the observed measurements was calculated. Once all the pressures were tested, the deviation between the PNT readings and the recorded measurements was plotted graphically. This comprehensive validation process aimed to assess the accuracy and reliability of the PNT in measuring and tracking the air volume accurately during different pressure conditions.

3.2.   Validation Codes

In this section, we discussed the codes used for the validation process. These codes are similar to those described in the previous section and serve the purpose of ensuring accurate and reliable measurements. In terms of firmware, which refers to the code written in the Arduino IDE, the main modification introduced by the firmware explained in 2.6 pertains to the inclusion of a cycle counter. This counter is responsible for keeping track of the number of breathing cycles completed. Once the counter reaches a value of 10, a
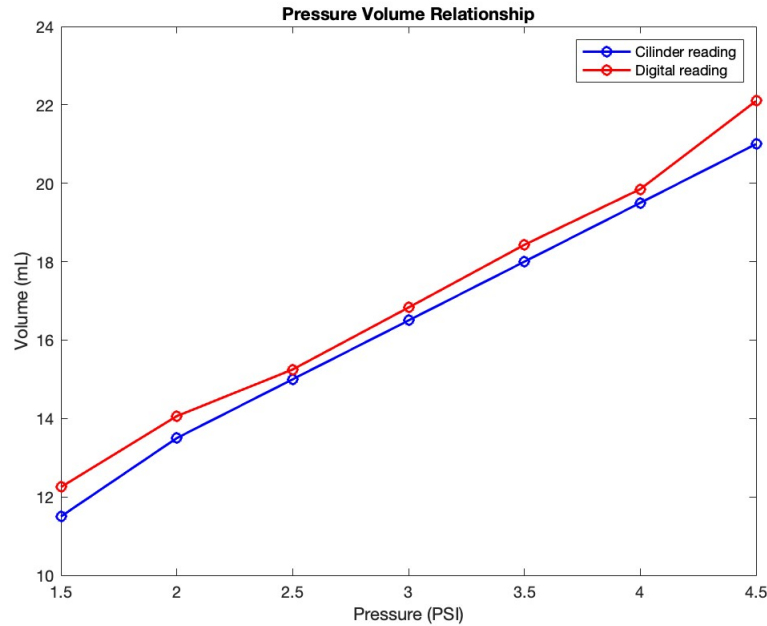
Figure 3.2: Pressure Volume Relationship: on x-axis pressure ranges, on y-axis Volume displacement after 10 cycles.

command is executed to shut off all the valves, effectively terminating the respiration process. On the other hand, in the Processing code, the innovation involves the accumulation of volumes over the course of these 10 breathing cycles. The purpose of this accumulation is to ensure synchronization between the measured water volume in the cylinder and the displayed volume in the user interface, ultimately contributing to a more robust validation process.

3.3.   Results of the PNT Validation

After conducting the experiment three times for each pressure range, the obtained values from the cylinder readings and the PNT were recorded and organized into a table. To ensure accuracy, the mean value was calculated for both sets of readings. Subsequently, the data were plotted using MATLAB, with the pressure values plotted along the x-axis in PSI, and the corresponding readings in milliliters (mL) plotted along the y-axis (Figure 3.2). Upon analyzing the graph, it becomes apparent that the readings obtained from the PNT tend to slightly overestimate the values observed from the cylinder. These observations and the potential underlying factors contributing to this discrepancy will be thoroughly discussed and examined in the upcoming Chapter 4, allowing for a comprehensive understanding of the results.

3.4.   Validation of Precise Timing for Valve Opening and Closing

In this section, a comprehensive evaluation was conducted to validate the precise timing of the firmware's instructions for opening and closing the valves. This validation process was of utmost importance, particularly when dealing with the administration of small volumes, as it aimed to ensure the accurate and safe delivery of the intended doses to the subject. The focus was on confirming that the valves were opened and closed for the exact duration specified in the firmware.

To assess the timing accuracy, an oscilloscope was employed as a reliable tool for capturing and analyzing the electrical signals sent to the valves. This allowed for precise monitoring of the duration during which the input signal to the valves remained in the high or low state. By comparing the observed timing data with the expected values specified in the firmware, it was possible to verify the correctness of the valve operation and ensure that the desired volumes were administered accurately. In the provided image, an oscilloscope is displayed, which is a highly useful electronic instrument used for visualizing and analyzing electrical signals. In this particular setup, one of the oscilloscope's probes is connected to the ground, which serves as the reference point, while the other probe is connected to the input of the valve in order to measure the signal.

By examining the first image (3.3), it is possible to observe the waveform of the signal. Specifically, we notice that the rising edge of the high signal occurs at a time interval of -240 ms, indicating the point at which the voltage transitions from a low value to a high value. Similarly, in the second image (3.4), the falling edge of the signal is observed at -91 ms, representing the moment when the voltage returns from a high value to a low value. The temporal span between these two edges corresponds precisely to a duration of 149 ms, which signifies the exact period during which the valve must remain open during the inspiration phase.
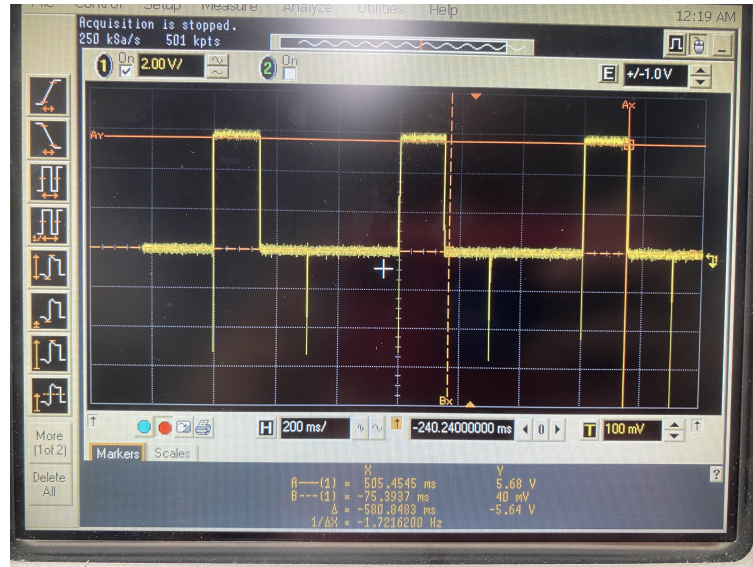
Figure 3.3: Signal waveform at time 240ms.
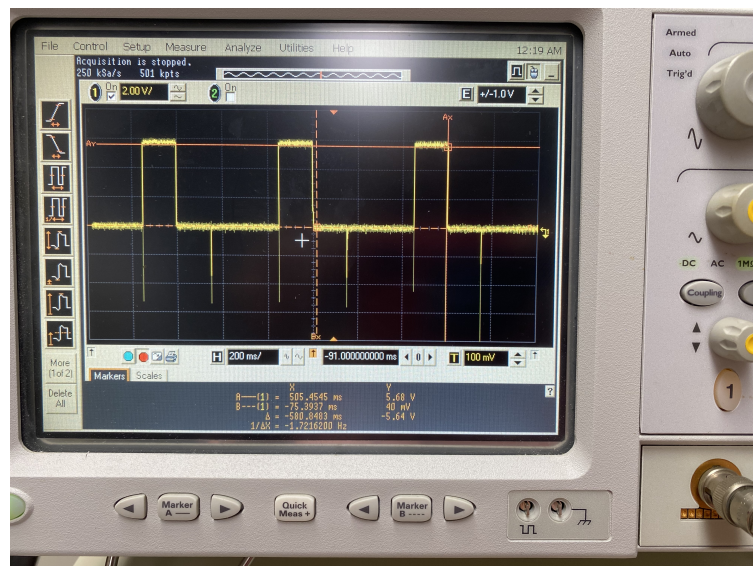
Figure 3.4: Signal waveform at time 91ms.

4 | Discussions

In this chapter, a comprehensive discussion of the validation process and the obtained results is presented. Firstly, the limitation introduced by the absence of flow restrictors will be addressed in Section 4.1, examining the implications it entails. Subsequently, the issue of integrating volume from the flow will be discussed in Section4.2, exploring the challenges and considerations associated with this matter.

4.1. Set-Up Limitation

As previously mentioned, the utilization of flow restrictors holds significant importance in the context of mechanical ventilation. In the study conducted by Nouls et al. on ventilators [16], flow restrictors with an impedance of 1250 cmH2O s/ml were utilized, while the impedance of the tubing was measured to be 85 cmH2O s/ml. It is worth noting that the impedance of the lungs can vary, ranging from 0.5 cmH2O s/ml under normal conditions to 2 cmH2O s/ml during bronchoconstriction [21].

The high resistance provided by flow restrictors renders the resistances of the tubing and the lungs comparatively negligible. As a consequence, the control and regulation of tidal volume predominantly rely on the resistance introduced by the flow restrictor, remaining unaffected by the impedance of the connecting tubing or any variations in lung impedance during imaging. Furthermore, flow restrictors play a critical role in maintaining the desired pressure and volume levels during the respiratory cycle. By exerting controlled resistance, they enable precise control of ventilation parameters, including inspiratory and expiratory flow rates, thus facilitating the delivery of appropriate respiratory support to the patient.

Therefore, in the absence of flow restrictors, the resistance introduced by the tubing became significant, particularly when working with very small flow volumes. This was evident in the variability of measurements observed from day to day, with slight variations in the cylinder volumes, such as an additional 2 mL every 10 cycles. When dealing with mice that require very small tidal volumes, this variability poses a considerable problem. The lack of flow restrictors leads to inconsistent and unpredictable delivery of tidal volume,

making it challenging to maintain precise control over ventilation parameters, which is crucial for experimental accuracy and animal welfare.

4.2.   Volume Drift

Another recurrent issue in the context of mechanical ventilators is the problem of flow integration, which leads to volume drift. Due to the inherent limitations of measurement instruments, achieving 100% precision is not feasible, and a finite offset is always present. As this offset is integrated over time, it results in a linear drift in volume, with a slope equal to the offset. The image representing the user interface shows a slight slope at the end when the flow is zero 2.50. The problem becomes more severe with prolonged usage of the flow meter.

During this thesis, attempts were made to address the issue by implementing a software filter that would remove the DC offset. However, this significantly slowed down the real-time volume calculation. Achieving accurate delineation of the zero flow point poses challenges, especially as the sensitivity of the pressure sensing element decreases, typically occurring as the linear range of measurement increases. Additionally, the resolution of the analog-to-digital converter used for flow sampling sets a limit on the accuracy of identifying the zero flow point. Consequently, achieving perfect offset compensation is not attainable. The problem becomes more severe with prolonged usage of the flow meter, As a resolution, at the end of each cycle, the volume is set to zero.

In summary, the problem of volume drift caused by flow integration is a common challenge in mechanical ventilators. Despite attempts to mitigate it through software filters, perfect offset compensation is unachievable due to inherent instrument limitations and the sensitivity range of pressure sensors.

5 | Conclusions and Future Developments

This thesis project represents an initial step towards a broader undertaking aimed at utilizing ^{129}Xenon Magnetic Resonance Elastography (MRE) to acquire information about the mechanical properties of the lungs, specifically lung stiffness. By developing a functional mechanical ventilator system and integrating advanced imaging techniques, researchers aim to enhance our understanding of lung mechanics and improve patient care in respiratory medicine.

Therefore, the achievements of this project encompassed several key objectives:

- Extensive review of literature on commercially available mechanical ventilators.

- Meticulous selection of components based on research, technical specifications, compatibility, and reliability.

- Design and development of 3D components for constructing the ventilator box using Solidworks.

- Establishment of hardware connections to enable seamless communication and interaction between components and subsystems.

- Development of software capable of executing hardware commands, and adjusting ventilation parameters.

- Development of a user interface providing real-time monitoring of vital parameters and results.

- Calibration and validation of the pressure and flow sensing device (PNT) for accurate monitoring of tidal volume.

Indeed, since it is only the beginning of the project, there is a significant amount of work to be done. Here is a detailed breakdown of the tasks involved:

1. Repeat Experiments with PNT and Restrictors:

- Once the flow restrictors are received, it is necessary to repeat the experiments conducted with the flowmeter sensing device (PNT).

- For each pressure range, measure the obtained volume, both with the reading on the user interface and both with the immersed cylinder, to determine the appropriate initial gas pressure settings for achieving the desired tidal volume.

- This validation ensures that the ventilator can accurately deliver the intended tidal volume under various pressure conditions

2. Perform Phantom Testing:

   - Represent the lungs of a mouse as an RC (resistance-compliance) system with a resistance of 0.573 cmH2O*s/ml and Compliance of 0.069 ml/cmH2O.

   - Use a stainless surgical needle (G18, 3.8cm length, 0.838mm internal diameter) and a 100ml glass bottle to simulate the lung properties.

   - Conduct tests on the phantom to evaluate the ventilator's ability to deliver appropriate pressure and volume changes, replicating the behavior of a mouse's lungs.

3. Hardware Implementation:

   - Develop a PCB (Printed Circuit Board) with all the necessary components to establish permanent connections and prevent wire disconnections.

4. Assemble the Ventilator Box:

   - Assemble all the components into the ventilator box, ensuring proper organization.

5. Test the Ventilator in the MRI Room:

   - Conduct thorough testing of the ventilator inside the MRI chamber to ensure its compatibility and functionality within the specific environment.

6. Develop Animal Testing:

   - Once the preliminary testing and validation are completed, proceed to the animal testing phase.

In summary, the following stages of the project involve repeating experiments with the PNT and restrictors, validating the ventilator's performance, conducting phantom testing, implementing the PCB board, assembling the ventilator box, testing it in the MRI

chamber, and finally, progressing to animal testing. Each step contributes to the overall goal of developing the mechanical ventilator system suitable for ^{129}Xenon MRE research.

Bibliography

[1] T. S. Blackwell, A. M. Tager, Z. Borok, B. B. Moore, D. A. Schwartz, K. J. Anstrom, Z. Bar-Joseph, P. Bitterman, M. R. Blackburn, W. Bradford, et al. Future directions in idiopathic pulmonary fibrosis research. an nhlbi workshop report. *American journal of respiratory and critical care medicine*, 189(2):214–222, 2014.

[2] M. A. Dresner, G. H. Rose, P. J. Rossman, R. Muthupillai, A. Manduca, and R. L. Ehman. Magnetic resonance elastography of skeletal muscle. *Journal of Magnetic Resonance Imaging: An Official Journal of the International Society for Magnetic Resonance in Medicine*, 13(2):269–276, 2001.

[3] A. Dutt and K.-K. Wong. Mouse models of lung cancer. *Clinical cancer research*, 12 (14):4396s–4402s, 2006.

[4] F. Fakhouri, S. Kannengiesser, J. Pfeuffer, Y. Gokun, and A. Kolipaka. Free-breathing mr elastography of the lungs: An in vivo study. *Magnetic resonance in medicine*, 87(1):236–248, 2022.

[5] B. Goss, K. P. McGee, E. Ehman, A. Manduca, and R. Ehman. Magnetic resonance elastography of the lung: technical feasibility. *Magnetic Resonance in Medicine: An Official Journal of the International Society for Magnetic Resonance in Medicine*, 56 (5):1060–1066, 2006.

[6] J. T. Grist, M. Chen, G. J. Collier, B. Raman, G. Abueid, A. McIntyre, V. Matthews, E. Fraser, L.-P. Ho, J. M. Wild, et al. Hyperpolarized 129xe mri abnormalities in dyspneic patients 3 months after covid-19 pneumonia: preliminary results. *Radiology*, 301(1):E353–E360, 2021.

[7] N. Hirota and J. G. Martin. Mechanisms of airway remodeling. *Chest*, 144(3):1026–1032, 2013.

[8] R. M. A. K. Huiming Dong, Rizwan Ahmad. Mr elastography inversion by compressive recovery. *Physics in Medicine Biology*, 66(16):165001, 2021.

[9] H. Imai, H. Matsumoto, E. Miyakoshi, S. Okumura, H. Fujiwara, and A. Kimura.

Regional fractional ventilation mapping in spontaneously breathing mice using hyperpolarized 129xe mri. *NMR in Biomedicine*, 28(1):24–29, 2015.

[10] H.-U. Kauczor, R. Surkau, and T. Roberts. Mri using hyperpolarized noble gases. *European radiology*, 8:820–827, 1998.

[11] J. Kemper, R. Sinkus, J. Lorenzen, C. Nolte-Ernsting, A. Stork, and G. Adam. Mr elastography of the prostate: initial in-vivo application. In *RöFo-Fortschritte auf dem Gebiet der Röntgenstrahlen und der bildgebenden Verfahren*, volume 176, pages 1094–1099. © Georg Thieme Verlag KG Stuttgart· New York, 2004.

[12] J. F. Mata, T. A. Altes, J. Cai, K. Ruppert, W. Mitzner, K. D. Hagspiel, B. Patel, M. Salerno, J. R. Brookeman, E. E. De Lange, et al. Evaluation of emphysema severity and progression in a rabbit model: comparison of hyperpolarized 3he and 129xe diffusion mri with lung morphometry. *Journal of applied physiology*, 102(3): 1273–1280, 2007.

[13] P. J. McCracken, A. Manduca, J. Felmlee, and R. L. Ehman. Mechanical transient-based magnetic resonance elastography. *Magnetic Resonance in Medicine: An Official Journal of the International Society for Magnetic Resonance in Medicine*, 53(3): 628–639, 2005.

[14] H. E. Möller, X. J. Chen, B. Saam, K. D. Hagspiel, G. A. Johnson, T. A. Altes, E. E. de Lange, and H.-U. Kauczor. Mri of the lungs using hyperpolarized noble gases. *Magnetic Resonance in Medicine: An Official Journal of the International Society for Magnetic Resonance in Medicine*, 47(6):1029–1051, 2002.

[15] R. Muthupillai, D. Lomas, P. Rossman, J. F. Greenleaf, A. Manduca, and R. L. Ehman. Magnetic resonance elastography by direct visualization of propagating acoustic strain waves. *science*, 269(5232):1854–1857, 1995.

[16] J. Nouls, M. Fanarjian, L. Hedlund, and B. Driehuys. A constant-volume ventilator and gas recapture system for hyperpolarized gas mri of mouse and rat lungs. *Concepts in Magnetic Resonance Part B: Magnetic Resonance Engineering*, 39(2):78–88, 2011.

[17] F. Peeters, R. Sinkus, N. Salameh, L. Annet, L. terBeek, and B. VanBeers. In vivo mr-elastography of liver fibrosis. In *ISMRM 13th Scientific Meeting & Exhibition*, number CONF, 2005.

[18] N. S. Shah, S. A. Kruse, D. J. Lager, G. Farell-Baril, J. C. Lieske, B. F. King, and R. L. Ehman. Evaluation of renal parenchymal disease in a rat model with magnetic

resonance elastography. *Magnetic Resonance in Medicine: An Official Journal of the International Society for Magnetic Resonance in Medicine*, 52(1):56–64, 2004.

[19] E. E. Van Houten, M. M. Doyley, F. E. Kennedy, J. B. Weaver, and K. D. Paulsen. Initial in vivo experience with steady-state subzone-based mr elastography of the human breast. *Journal of Magnetic Resonance Imaging: An Official Journal of the International Society for Magnetic Resonance in Medicine*, 17(1):72–85, 2003.

[20] R. S. Virgincar, J. Dahlke, S. H. Robertson, N. Morand, Y. Qi, S. Degan, B. Driehuys, and J. C. Nouls. A portable ventilator with integrated physiologic monitoring for hyperpolarized 129xe mri in rodents. *Journal of Magnetic Resonance*, 295:63–71, 2018.

[21] S. Wagers, L. Lundblad, H. T. Moriya, J. H. Bates, and C. G. Irvin. Nonlinearity of respiratory mechanics during bronchoconstriction in mice with airway inflammation. *Journal of Applied Physiology*, 92(5):1802–1807, 2002.

[22] T. Wakayama, T. Ueyama, F. Imai, A. Kimura, and H. Fujiwara. Quantitative assessment of regional lung ventilation in emphysematous mice using hyperpolarized 129xe mri with a continuous flow hyperpolarizing system. *Magnetic Resonance Imaging*, 92:88–95, 2022.

[23] C.-S. Wu, H.-C. Chou, L.-T. Huang, C.-M. Lin, Y.-K. Lin, and C.-M. Chen. High amplitude bubble continuous positive airway pressure decreases lung injury in rats with ventilator-induced lung injury. *Journal of the Chinese Medical Association*, 82 (10):795–801, 2019.

List of Figures

Acknowledgements

I would like to express my gratitude to Dr. Thomas J. Royston, without whose invaluable ideas, direction, and support the project wouldn't have been possible. I would like to express my heartfelt gratitude to Django, who worked alongside me during these months to bring this project to fruition. I am immensely thankful to all my colleagues in the lab, especially Marta, Irene, and Aime, who provided invaluable suggestions and support throughout the journey. I would also like to extend my gratitude to Weiguo Li for his expert advice on the MRI specifications, which greatly contributed to the success of this project.

I am deeply appreciative of Professor Dellacà and Davide Bizzotto for their unwavering availability and assistance, guiding me step by step in the development of the device. Their expertise and mentorship have been instrumental in shaping the outcome of this project.

To my parents, whose unwavering support and belief in me have brought out the best in me. They have always encouraged me and provided the foundation for the person I am today. I am also grateful to my brother and my entire family, especially my aunt Lolita, who have consistently shown me unconditional love and support.

Lastly, I extend my gratitude to my friends, both longstanding and newfound, who have been a constant source of comfort and have stood by my side during the various challenges I have faced.